Characterization and Modeling of Spatial Variability in a Complex Alluvial Aquifer: Implications on Solute Transport

Alexander Y. Sun[1] (asun@swri.org)
Robert W. Ritzi[2]
Darrell W. Sims[3]

[1] Center for Nuclear Waste Regulatory Analyses, Geosciences and Engineering Division, Southwest Research Institute®, San Antonio, TX
[2] Department of Earth and Environmental Sciences, Wright State University, Dayton, OH
[3] Department of Earth, Material, and Planetary Sciences, Geosciences and Engineering Division, Southwest Research Institute®, San Antonio, TX

Abstract

Field investigations of stratified alluvial deposits suggest that they can give rise to a hierarchy of permeability modes across scales, corresponding to a hierarchy of sedimentary unit types and thus may lead to enhanced plume spread in such media. In this work, we model the sedimentary architecture of the Quaternary alluvium of Fortymile Wash, Nevada, using a hierarchical transition probability geostatistical approach. The alluvial aquifer comprises a segment of the groundwater flow pathway from the potential high-level nuclear waste repository at Yucca Mountain, Nevada to the downstream accessible environment and is considered an important component of the saturated zone because of its potential to retard radionuclide migration significantly. Thus, our main goal is to quantify the impact of flow path heterogeneity on radionuclide transport in the alluvium by explicitly accounting for the spatial variability of hydrofacies distributions within the alluvial aquifer. The alluvial aquifer is a gravel-dominated, braid-belt deposit, having lower-permeability paleosols interstratified with higher-permeability gravel-bar deposits. A quantitative, three-dimensional, two-level hierarchical model of alluvium spatial variability is developed through fusion of multiple geologic data types and sources on the one hand and scaling relationships established from modeling similar depositional environments on the other. Markov chain models of unit type transition probabilities are employed to represent complex patterns of spatial variability at each hierarchical level in a geostatistical fashion and to impose realistic constraints to such variations through conditioning on existing data. Finally, we demonstrate the link between the alluvium spatial variability and solute dispersion at different spatiotemporal scales using macrodispersion coefficients established in the stochastic-Lagrangian transport theory. Our numerical experiments for nonreactive solutes, based partly on data derived from Fortymile Wash alluvial aquifer, suggest that the longitudinal macrodispersivity can be on the order of hundreds to thousands of meters, and its asymptotic value is not reached until after 1,000 years.

1. Introduction

Yucca Mountain, Nevada, has been identified by the U.S. Department of Energy (DOE) as a potential high-level nuclear waste repository site. A critical performance requirement for Yucca Mountain is that it must include both natural and engineered barriers [10 CFR 63.113(a)]. The saturated zone below Yucca Mountain constitutes the most likely pathway for radionuclides to reach the accessible environment and is expected to act as a natural barrier to radionuclide transport. To assess the efficacy of the saturated zone in delaying radionuclide transport and reducing the concentrations of radionuclides before they reach the accessible environment, appropriate characterization and understanding of the saturated zone is necessary.

Groundwater in the Yucca Mountain vicinity is conceptualized as flowing southerly from recharge areas at higher elevations north and northwest of Yucca Mountain, coalescing in the Fortymile Wash valley-fill alluvial aquifer, and flowing toward the Amargosa desert (Figure 1). The average groundwater velocity in the alluvial aquifer is significantly lower as compared to that in the upgradient volcanic tuff units, and the higher mineral surface area of alluvial materials is expected to contribute to greater sorption in the alluvium [Bechtel SAIC Company, LLC, 2004d; U.S. Nuclear Regulatory Commission (NRC), 2005]. DOE and NRC have developed a series of site-scale models to describe the geology of the saturated zone and characterize flow and transport processes within it (Bechtel SAIC Company, LLC, 2004a–c; Winterle, 2003; Farrell, et al., 2005). The geohydrologic properties of the alluvial aquifer are assumed homogeneous in the current DOE and NRC site-scale saturated zone models.

The main goal of this study is to model the spatial variability within the Fortymile Wash alluvial aquifer and to assess the implication of flow path heterogeneity on potential radionuclide transport. We seek a parsimonious, quantitative, three-dimensional representation of heterogeneity that captures the aspects of sedimentary architecture relevant to mass transport. A model representing higher- and lower-permeability hydrofacies is used to characterize the complexity of transport pathways through the alluvium and to characterize the resulting complexity in transport residence times within the Fortymile Wash alluvial aquifer.

Previous studies have described the textures, depositional environment, and sedimentary architecture of the Fortymile Wash alluvium (Ressler, et al., 2000; Potter, et al., 2002). The alluvium is a gravel-dominated deposit, having lower-permeability paleosols interstratified with higher-permeability braid-belt deposits. Thus, a conceptual model exists for the heterogeneity within the saturated alluvium (i.e., hydrofacies types and their sedimentary architecture). However, current site-specific transport models do not yet explicitly represent such heterogeneity. This may be in part because the available sources of data reflecting local conditions (e.g., outcrop exposure maps, borehole drilling records, and geophysical data) are viewed as coming from too few locations too far apart, and thus the data are deemed insufficient for developing a model at the aquifer-wide scale. In fact, this could be stated as a problem common to many sites.

Though the saturated alluvium is sparsely sampled, we can still create a useful model by adopting a stochastic modeling framework. We develop a methodology to quantify the uncertainty in the interpolation of strata between data locations by defining probabilities of stratal occurrence within the three-dimensional model domain. We are more interested in representing general transport characteristics of the heterogeneous saturated alluvium package on the whole than in accuracy at any one specific location. Accordingly, though we quantify uncertainty at specific locations, we focus on requiring that the modeling approach honor the salient features of the conceptual model for hydrofacies and sedimentary architecture over the region of the model domain. Furthermore, we require that the approach honor the geometric measures (proportions, mean lengths, and juxtapositional relationships) of strata that have been quantified from data locations and honor stratal occurrence at locations where data do exist. In meeting these requirements, our methodology leads to a spatial variability model that is, from the perspective of the bulk alluvial package, both geologically defensible and useful in a stochastic framework.

There is a rich literature on methods for stochastic modeling of aquifer architecture. Geostatistical approaches based on facies indicator spatial random functions have proven to be useful (e.g., Rubin, 1995; Carle and Fogg, 1996, 1997; Weissman and Fogg, 1999; Lu and Zhang, 2002; Ritzi, et al., 2004; Dai, et al., 2005; and Rubin, et al., 2006). We adopt elements from them in our methodology. These are elements of

probability theory that provide the general mathematical framework for defining the spatial probability of stratal occurrence. What is new in our methodology is the fusion of many types and sources of data within the framework to define the spatial probabilities for stratal occurrence and to simulate and represent the sedimentary architecture. Multiple data sources and types reinforce the applicability of a conceptual model by their consistency in documenting the occurrence of the same strata in the same relative abundance. Furthermore, like different pieces of a puzzle, each data type fits together, providing different, complementary metrics that we require for modeling the "whole picture" of the Fortymile Wash alluvial aquifer.

The organization of this paper is as follows. Section 2 provides background information about Fortymile Wash and its surroundings. Section 3 lays out the general framework of transition probability and Markov chain approach and delineates our methodology for modeling the Fortymile Wash sedimentary architecture by fusing multiple data sources. Section 4 presents the results of our analyses. Finally, discussion and conclusions are given in Section 5.

2. Physiography and Geology

Fortymile Wash, a topographic feature and an inferred structural trough, is the largest tributary of the upper Amargosa River and one of the largest alluvial systems in the southern Basin and Range Province (Lundstrom, et al., 1998). Fortymile Wash is physiographically bounded to the west by Yucca Mountain; to the north by the Calico Hills; to the east by Jackass Flats, Little Skull Mountain, and the Striped Hills; and extends southward to merge with Amargosa Desert (Figure 1). Potter, et al. (2002) observed that sedimentologic properties of the various alluvial units in the vicinity of Yucca Mountain are very similar: fluvial deposits are predominantly sandy gravel with interbedded gravely sand and sand. Fluvial facies present in these deposits include coarse-grained channel bars and intervening finer-grained swales. The mafic lavas are the main source of the mafic clasts in the Quaternary alluvium (Lundstrom and Warren, 1994).

The modern Fortymile Wash channel is entrenched to depths exceeding 20 m and gently grades into a wide braid plain within the Amargosa Desert (Figure 1). Soils of the

fan surface flanking the entrenched segment of Fortymile Wash are interpreted from thermoluminescence and Uranium-series dates to be 40,000–60,000 years old, and the oldest terrace inset within the entrenchment is dated at 24,000–36,000 years (Lundstrom, et al., 1998). In the deeply incised upper portion of Fortymile Wash, deposits in the channel walls show interbedded fan and gravelly fluvial deposits (Lundstrom, et al., 1998; Ressler, et al., 2000).

3. Methodology

3.1. Characterizing, modeling, and simulating heterogeneity using the Markov chain approach

We now define our methodology for characterizing, modeling, and simulating the sedimentary architecture of Fortymile Wash alluvium using transition probability and the Markov chain approach. First, some definitions are necessary to facilitate further discussion. Consider that the sediment can be delineated into mutually exclusive region types that we will refer to here in the most general terminology as facies. A facies indicator spatial random function $I_i(\mathbf{x})$ is defined as

$$I_i(\mathbf{x}) = \begin{cases} 1 & \text{if facies type } i \text{ occurs at location } \mathbf{x} \\ 0 & \text{otherwise} \end{cases} \tag{1}$$

By definition, $\sum_i^M I_i(\mathbf{x}) = 1$ for any $\mathbf{x}$, where M is the total number of facies types in a facies assemblage. The volumetric proportion of the ith facies type p_i, is the probability that $I_i(\mathbf{x})$ is equal to 1, namely, $p_i = \Pr[I_i(\mathbf{x}) = 1]$. The transition probability measures the probability of transitioning from one facies type to another. Mathematically, this is the conditional probability of facies type j occurring at location $\mathbf{x} + \mathbf{h}_\phi$, given that facies type i occurs at location $\mathbf{x}$ (Carle and Fogg, 1996, Eq. 2.6)

$$t_{ij}(\mathbf{x}, \mathbf{x} + \mathbf{h}_\phi) = \Pr\left[I_j(\mathbf{x} + \mathbf{h}_\phi) = 1 \middle| I_i(\mathbf{x}) = 1\right] = \frac{\Pr\left[I_j(\mathbf{x} + \mathbf{h}_\phi) = 1, I_i(\mathbf{x}) = 1\right]}{\Pr\left[I_i(\mathbf{x}) = 1\right]} \tag{2}$$

where $\mathbf{h}_\phi$ is the separation vector between two spatial locations in the ϕ direction, and $\Pr\left[I_j(\mathbf{x} + \mathbf{h}_\phi) = 1, I_i(\mathbf{x}) = 1\right]$ is the joint probability for j-th facies to occur at $\mathbf{x} + \mathbf{h}_\phi$ and i-th facies to occur at $\mathbf{x}$.

Let $l_{i,\phi}$ be the length of the individual occurrence of facies type *i* along direction ϕ; the mean length $\bar{l}_{i,\phi}$ is defined as the total length of *i* divided by the total number of occurrences of *i* along ϕ. Carle and Fogg (1996) showed that $\bar{l}_{i,\phi}$ is related to the value of the derivative of the autotransition probability at zero lag

$$\bar{l}_{i,\phi} = -\left[\partial t_{ii}(h_\phi = 0) / \partial h_\phi\right]^{-1} \tag{3}$$

where h_ϕ is the magnitude of $\mathbf{h}_\phi$.

Spatial variability in facies distributions can be modeled by interpolating one-dimensional Markov chain models for the principal directions (Lin and Harbaugh, 1984; Carle and Fogg, 1997). A one-dimensional continuous-lag Markov chain model assumes that the outcome at a location $\mathbf{x} + \mathbf{h}_\phi$ depends only on location **x** and is given by the following matrix exponential (Carle and Fogg, 1997)

$$\mathbf{T}(h_\phi) = \exp(\mathbf{R}h_\phi) \tag{4}$$

where **T** is a transition probability matrix whose entries are defined in Eq. (2), and **R** is a transition rate matrix whose entries r_{ij} represent the rate of change from facies type *i* to *j* per unit length in ϕ. Eq. (3) shows that the diagonal terms of **R** are related to the mean lengths as

$$r_{ii,\phi} = -\frac{1}{l_{i,\phi}} \tag{5}$$

Entries of **R** must satisfy the following constraints (Carle and Fogg, 1997)

$$\sum_j^M r_{ij} = 0, \forall i, \text{and}$$

$$\sum_i^M p_i r_{ij} = 0, \forall j \tag{6}$$

The identities in Eq. (6) imply that only the transition rates of *M*-1 facies types need to be calculated for a system consisting of *M* facies types. The transition rates of the background facies, usually chosen to be the most dominant category that fills in the space not occupied by other categories, can be inferred using Eq. (6). In case of two-facies or bimodal models (e.g., Desbarats, 1990; Rubin, 1995; Ritzi, 2000), the transition rate matrix is completely defined by specifying a diagonal term. Thus, the proportion and

(statistical) geometry need only be known for one facies type. The Markov chain model is an extremely powerful tool in these cases (Carle, et al., 1998; Ritzi, 2000; Rubin, et al., 2006).

Univariate statistics such as volumetric proportions, as well as mean lengths in the vertical and lateral directions, are needed to construct Markov chain models of transition probabilities. Modeling unit type distributions in lateral directions is usually the most challenging aspect of applying the transition probability geostatistics, largely because of the lack of borehole spatial coverage and other secondary information in lateral directions.

The first step toward developing the Markov model, in our approach, is to use geologic information about the unit types present and the processes of deposition that created them. The goal is to have a conceptual model for the sedimentary architecture to guide the model development. We use studies of outcrop exposures of unsaturated alluvium for this purpose (Ressler, et al., 2000). Outcrop exposures facilitate quantifying textural attributes of the sediment, classifying the sediment types present, delineating stratigraphy, mapping stratal boundaries, interpreting depositional environments, and quantifying geometric attributes (especially thickness) and juxtapositioning relationships (especially in the vertical direction). Some unit types may terminate laterally within the exposure and thus facilitate developing estimates of lateral lengths, usually along only one azimuth. Exposures are often limited to providing a two-dimensional, vertical-plane perspective. Many of the strata extend beyond the limits of the exposure, and thus we require other methods for defining their lateral lengths.

Evidence must be provided to support that the exposures of sediment are representative of saturated sediments deeper below the water table. We use drillers' lithologic logs from Nye County Early Warning Drilling Program (EWDP), an ongoing investigation whose goals are to better understand flow paths from the potential Yucca Mountain repository and to establish a local ground monitoring system (Nye County Nuclear Waste Repository Office, 2007). Two EWDP boreholes have been drilled using the rotosonic (or sonic) coring method (Nye County Nuclear Waste Repository Project Office, 2005). Rotosonic coring provides large-diameter, high-quality core sampling for use in sediment identification. Continuous core is readily taken from below the water

table, and textural attributes of the sediment (grain size, sorting) can be quantified from the core. Quantification of textural attributes in the core, below the water table, can be compared to quantifications of sediment texture in outcrop exposures above the water table. The comparison provides a basis for deciding whether outcrop exposures serve as analogs.

There typically are only a small number of sonic cores drilled at a given site, so there is limited information about lateral continuity of strata in sonic core data. Logs of borehole cuttings are usually available from a greater number of locations than sonic cores and can be used to broaden the spatial coverage of lithologic data (Nye County Nuclear Waste Repository Project Office, 2005). Skilled drillers or technicians can infer sediment types from cuttings strained from the drilling fluid and the resistance to bit advancement by comparing the logs; the reliability of cutting logs can be assessed where rotary holes have been drilled adjacent to rotosonic holes. The textural descriptions are not as reliable as those recorded from a sonic core, but often reflect the larger textural changes with depth and can be used to vertically delineate significant unit types. Logs of borehole resistivity through the saturated subsurface provide an indication of electronegativity of mineral types within the sediment. Resistivity logs are especially useful for determining the presence of clay minerals within the sediment and thus can be used as support for the interpretation of clay sediment in cutting logs. If reliable, cutting logs are useful for assessing the applicability of the conceptual model(s) for heterogeneity developed in outcrop studies over broader regions of the saturated subsurface. Where the conceptual model is supported, the cutting logs are useful for broadening estimates of the thickness of unit types. If abundant and not clustered, they are also useful in broadening the estimates of stratal proportions. Together, these analyses allow for the assessment of the spatial stationarity of the conceptual model.

Boreholes from which cutting logs are collected are almost always too far apart to satisfactorily quantify lateral lengths or indicator correlation scales (Proce, et al., 2004). Recent studies of modern fluvial deposition have provided universal scaling relationships for the dimensions of fluvial bedforms as a function of channel width. Furthermore, they have provided scaling relationships for the ratio of the lateral length to the thickness of strata as a function of the fluvial bedform geometries (Lunt, et al., 2004; Rubin, et al.,

2006). If the fluvial depositional environment is identified from outcrop studies, along with the width of channels and the thickness of sedimentary unit types, then the scaling relationships can be used to assess the average lateral length of unit types on an order-of-magnitude basis. This approach meets the requirements for representing the alluvial package on the whole and producing a geologically defensible model.

In Section 4, we illustrate how each of these sources of information about sedimentary architecture leads to a geologically defensible form of Eq. (4), the continuous-lag Markov chain model. Once the Markov model is defined, it is particularly useful in generating realizations of the alluvial sedimentary architecture through sequential indicator simulation with quenching (Carle, 1999).

The TProGS package developed by Carle (1999) uses a sequential indicator simulation algorithm to generate an initial configuration, where the local facies type probabilities are estimated conditional to nearby data and already simulated cells. Thus, for each grid cell, the probability of occurrence of a facies type k is approximated by

$$\Pr(k \text{ occurs at } \mathbf{x} \left| I_j(\mathbf{x}_\alpha); \alpha = 1,...,N; j = 1,...,M \right.) \approx \sum_{\alpha=1}^{N} \sum_{j=1}^{M} I_j(\mathbf{x}_\alpha) w_{jk,\alpha} \qquad (7)$$

where N is the number of data, M is the number of facies types, and $w_{jk,\alpha}$ are weighting coefficients determined by solving a transition probability-based cokriging system of equations. The sequential indicator simulation algorithm alone does not adequately reproduce the spatial variability prescribed by the Markov chain model. A simulated quenching step is followed to improve the match between modeled and simulated spatial variability. The quenching step is important in generating realizations that honor the mean lengths implied in the Markov chain model. The geological model simulated using TProGS can be used as input for flow and transport modeling. To create heterogeneity at small scales (cm-scale in this work) would require a high-resolution numerical grid, which is beyond what is practical for groundwater flow and transport models at the field scale. As a result, upscaling is typically performed to coarsen the grid resolution so that the flow and transport modeling becomes tractable (see Farmer, 2002, and de Marsily, et al., 2005, for recent reviews).

3.2. Macrodispersion in hierarchical architecture of deposits

As an alternative to brute-force numerical simulation, the stochastic-Lagrangian theory for subsurface transport, especially the macrodispersion concept, provides a way of assessing the effect of porous media heterogeneity on solute transport. The Lagrangian approach considers displacement of solute particles over time. The effect of spatial variability on solute transport can be characterized through relating permeability variability to solute particle displacement statistics, from which macrodispersion coefficients are derived. The concept of macrodispersion was originally introduced to explain the scale dependence of transport behavior at the field scale (Dagan, 1989). Relative contributions of the different types of spatial variability on solute transport at different time scales can be assessed via studying the pre-asymptotic behavior of macrodispersion coefficients.

Rubin (1995) derived analytical expressions for macrodispersion coefficients for statistically stationary bimodal formations, where the domain was assumed unbounded and the flow field at steady-state and uniform in the mean. A closed-form expression of travel time variance was derived by Rubin (1995) using the macrodispersion coefficients and was shown to bound the travel time variances simulated numerically by Desbarats (1990) for strongly bimodal sand-shale sequences. Rubin (2003) and Ritzi, et al. (2004) considered correlation of permeability in high-order hierarchical sedimentary architectures, where the sedimentary deposit was envisioned as consisting of a hierarchy of sedimentary units that differ in scale, geometry, and orientation. The indicator function representation of Ritzi, et al. (2004) can be defined for a hierarchy of sedimentary unit types, with any number of unit types at each of any number of hierarchical levels.

We use macrodispersion coefficients to assess the value in representing different scales of unit types. Just as with the indicator simulation approach, sedimentary architecture is represented by the proportions and transition probabilities of strata. In the following, we limit ourselves to a two-level, two-unit-type hierarchical architecture, where at level I, the spatial variability results from two regions of different permeability modes within a facies type and at level II, from variability in juxtapositional relationships among two facies types.

Starting from level II, the log-hydraulic conductivity field is modeled using a hybrid spatial random function (Rubin, 1995, Eq. 1)

$$Y(\mathbf{x}) = \sum_{i=1}^{2} I_i(\mathbf{x}) Y_i(\mathbf{x}) \tag{8}$$

where $Y_i(\mathbf{x})$ (i = 1,2) stands for log-hydraulic conductivity of the *ith* facies. Assume that $Y_i(\mathbf{x})$ are uncorrelated, and the first two moments of $Y(\mathbf{x})$ for statistically stationary and isotropic media are (Rubin, 1995; Dai, et al., 2004)

$$m_Y = \langle Y \rangle = \sum_{i=1}^{2} p_i \langle Y_i \rangle = \sum_{i=1}^{2} p_i m_i$$

$$\sigma_Y^2 = \sum_{i=1}^{2} p_i \sigma_{Y,i}^2 + \frac{1}{2} \sum_{i=1}^{2} \sum_{i \neq j} p_i p_j (m_i - m_j)^2$$

$$C_Y(h) = \sum_{i=1}^{2} p_i C_{Y,i}(h) t_{ii}(h) + \frac{1}{2} \sum_{i=1}^{2} \sum_{i \neq j} p_i (p_j - t_{ij}(h))(m_i - m_j)^2 \tag{9}$$

where $\langle \cdot \rangle$ is the expectation operator, the symbols m, σ^2, and C denote the mean, variance, and auto-covariance of log-hydraulic conductivity, respectively, and the transition rates $t_{ij}(h)$ can be obtained from Eq. (2) for statistically isotropic media. In hierarchical sedimentary architectures, there can be less variability within facies types than between them because facies represent similar depositional processes and environments that produce similar products (Koltermann and Gorelick, 1996). We can define ρ as the ratio between geometric means of the high- and low-permeability facies in the current model [i.e., $\rho = \exp(m_2 - m_1)$ with index "1" corresponding to the low-permeability facies]. Dai, et al. (2004) show that under the condition of high contrast between the hydraulic conductivity of facies types (ρ>10), the variability within a facies type is dominated by the contrast across the facies types, and the variance and covariance in Eq. (9) can be approximated by (Dai, et al, 2004, Eq. 26)

$$\sigma_Y^2 \approx \frac{1}{2} \sum_{i=1}^{2} \sum_{j \neq i} p_i p_j (m_i - m_j)^2 = p_1 p_2 (m_1 - m_2)^2 = p_1 p_2 (\ln \rho)^2$$

$$C_Y(h) \approx \frac{1}{2} \sum_{i=1}^{2} \sum_{j \neq i} p_i (p_j - t_{ij}(h))(m_i - m_j)^2 \tag{10}$$

As a result of the above approximation, σ_Y^2 becomes a linear function of $(\ln\rho)^2$ for fixed volumetric proportions.

Macrodispersion coefficients are derived from the velocity covariance, which ultimately, is related to the statistics of log-hydraulic conductivity shown above. The expressions for macrodispersion given by Rubin (1995) were for conservative solute transport in two-dimensional flows. Dai, et al. (2004) further generalized his results for conservative solute transport in three-dimensional flow and higher-order hierarchies based on the work of Ritzi, et al. (2004). Here we adopt the results of Dai, et al. (2004) for the case of high-contrast in log-hydraulic conductivities

$$\frac{D_L(t)}{U_1} = \sigma_Y^2 \lambda_I \left\{ 1 + \frac{4}{\exp(\tau)\tau^4} \left[6\left(\exp(\tau) - \tau - 1\right) - \tau^2 \left(\exp(\tau) + 2\right) \right] \right\} \tag{11}$$

$$\frac{D_T(t)}{U_1} = \sigma_Y^2 \lambda_I \left\{ \frac{1}{\exp(\tau)\tau^4} \left[12\left(1 + \tau - \exp(\tau)\right) + \tau^2 \left(5 + \exp(\tau) + \tau\right) \right] \right\} \tag{12}$$

where $D_L(t)$ and $D_T(t)$ are longitudinal and transverse (both transverse vertical and transverse horizontal) macrodispersion coefficients, respectively; t is elapsed travel time; U_1=constant is the mean groundwater velocity in the longitudinal direction; λ_I is the indicator correlation scale for transition probabilities; and $\tau = tU_1 / \lambda_I$. For the two-facies model considered here, the indicator correlation scale λ_I is defined as (Ritzi, 2000; Lu and Zhang, 2002)

$$\lambda_I = \bar{l}_{1,h} p_2 = \bar{l}_{2,h} p_1 \tag{13}$$

where $\bar{l}_{1,h}$ and $\bar{l}_{2,h}$ are the mean lengths of facies in the lateral directions. The quantity D/U, which has the same dimension as dispersivity, is called macrodispersivity. It is the rate of change of the second spatial moment of a plume. The large-time, asymptotic limits of macrodispersivities are obtained from Eqs. (11) and (12) as

$$\frac{D_L(t \to \infty)}{U_1} = \sigma_Y^2 \lambda_I = \frac{\lambda_I}{2} \sum_{i=1}^{2} \sum_{j \neq i} p_i p_j (m_i - m_j)^2$$

$$\frac{D_T(t \to \infty)}{U_1} = 0 \tag{14}$$

Ritzi (2000) showed that as the coefficient of variation for length in a particular direction becomes large, transition probabilities have an asymptotic, exponential like shape, and the effective ranges (a_{ii}, the abscissa at which 95% of the asymptote is reached) of autotransition probabilities tend toward

$$a_{ii} = 3\bar{l}_{ii}(1 - p_{ii}) \tag{15}$$

where p_{ii} and $\bar{l}_{ii}$ are volumetric proportion and mean length of facies *i*. If exponential models are used for all auto- and cross-transition probabilities among transitions from facies *i* to facies *j*, Dai, et al. (2005) showed that probability laws are enforced if

$$a_{ii} = a_{ij} = a_{jj} \tag{16}$$

The formulation of Dai, et al. (2004) requires that all auto- and cross-transition probabilities be exactly exponential and have equal effective ranges. In the following sections, a hierarchy of hydrofacies types will be developed for the Fortymile Wash alluvium. However, the effective ranges of the transition probabilities at different hierarchical levels are quite different. As a result, the Dai et al. (2004) formulation is not used; instead, we decouple the hierarchical levels and model them individually.

With the methodology and tools presented in this section, we can establish a hydrofacies model for Fortymile Wash deposits based on outcrop analog studies, augment the facies model further using both EWDP drillers' logs and literature studies, develop a three-dimensional Markov chain model of transition probabilities, and finally, quantify the effects of multimodal heterogeneity of the hierarchical sedimentary architecture using the concept of macrodispersion.

4. Application of methodology and results

4.1. A Fortymile Wash hydrofacies model developed from outcrop-analog studies

Ressler, et al. (2000) developed a conceptual model for heterogeneity within the saturated alluvium beneath Fortymile Wash. Sediments within the modern entrenched channel were studied and described from five laterally continuous, well-exposed outcrops. The locations of the outcrops are shown in Figure 2 (in small filled circles), and the picture of a representative outcrop exposure is shown in Figure 3. Eight diagnostic sedimentary facies (F1 to F8) were identified in their study based on grain size,

sedimentary structures, and geometry. These eight facies were, in turn, grouped into two categories based on permeability, forming two hydrofacies. These sedimentary facies and hydrofacies were later compared to a sonic core from 19PB and shown to represent the saturated alluvium (Stamatakos, personal communication, 2007[1]).

Here we further review the relevant details of classification of the sediments and hydrofacies model by Ressler, et al. (2000). This information is important for linking together the various sources of data that follow. The largest volume fraction of sediment was deposited within a gravel-dominated, braided-channel fluvial system. The most common and volumetrically significant facies consists of stratified sand and gravel in 30–50-cm-thick couplets, formed by longitudinal bar bedforms (sedimentary facies F1). Within fluvial braid-belt systems, most of the sediment indeed occurs and moves within longitudinal bars, which make up larger scale compound bars (braid bars and point bars). This F1 facies has open-framework gravels variably contained within the couplets. Four of the other sedimentary facies (F2, F3, F4, and F8), each occurring in smaller proportion, are related conglomerates, sandy gravels, and sands that formed in and around bar bedforms, including accumulation in cross-bar channels, confluence scour zones, and bar tops. These five sedimentary facies are grouped together as a relatively high-permeability hydrofacies. Occurrences of the high-permeability facies are on the order of 10 m thick. Two other sedimentary facies (F6, F7), both interpreted to be paleosols, include reddish, well-cemented sandstones and gravel-to-boulder calcrete horizons. The paleosols developed from pedogenic processes occurring on the tops of compound bars exposed between active channels and thus are laterally continuous for hundreds of meters, as are the bar deposits, though there may be local discontinuities. The carbonate cement and caliche give these sediments low permeability. The two paleosol facies are grouped together as a low-permeability facies. Occurrences of the low-permeability facies are on the order of 2 m thick. The remaining sedimentary facies (F5) was defined based on a single exposure that was grouped with the high-permeability hydrofacies. It is a sandy gravel deposited by gravity flows. It might be volumetrically larger in proximity to the slopes rimming Fortymile Wash. Figure 3 shows the exposure

[1] J. Stamatakos, CNWRA, Southwest Research Institute®, San Antonio, Texas, personal communication, 2007.

and measured section for one representative outcrop. The measured section can be subdivided into three occurrences of the braid-belt strata (high-permeability facies) separated by three occurrences of the paleosols (low-permeability facies). The high-permeability facies shows a laterally extensive tabular geometry with internal large-scale stratification. The low-permeability facies includes both thicker, more laterally extensive F7 units and locally discontinuous F6 units. The Nye County EWDP used the sonic coring method to extract intact large-diameter cores of the saturated alluvium in well 19PB, located south of the exposures along a line parallel to the axis of the valley (see Figure 2 for well locations). About 80 m of sonic core was collected. Examination of the 19PB core record suggests that it has two dominant lithofacies within the saturated alluvium zone (Stamatakos, personal communication, 2007[1]), both corresponding to braid-belt sedimentary facies that are grouped within the high-permeability facies category. One is facies F1, with well-organized 30–50-cm sand-gravel couplets, and the other is facies F4, with less-organized, more conglomeratic sandy gravel. These two most dominant facies in the core are the two most commonly documented in the measured sections from exposures of Fortymile Wash. The core in this zone also contains cemented red-colored sandstone intervals that are similar to the paleosol lithofacies described in the measured sections from Fortymile Wash (Walker, personal communication, 2007[2]). The consistency between the sediment in the core and in the measured sections offers evidence that the hydrofacies model developed from the outcrop study applies to the saturated alluvium.

4.2. Expanding the applicability of the hydrofacies model through analysis of cutting logs

Analysis of EWDP drillers' cutting logs gives additional support for the hydrofacies model established based on the outcrop analog studies and helps to quantify the volumetric proportions and geometric attributes of the hydrofacies. Our criteria in selecting EWDP wells to be included in this study are that the log must penetrate a significant interval within the saturated alluvium zone and must reflect the loggers'

[1]J. Stamatakos, CNWRA, Southwest Research Institute®, San Antonio, Texas, personal communication, 2007.
[2]J. Walker, Nye County Nuclear Waste Repository Project Office, Pahrump, Nevada, personal communication, 2007.

ability to detect the gravel (or larger) sediment. The water table in the vicinity of EWDP wells occurs around 700 m amsl, and the saturated alluvium is commonly at least 100 m thick. Thus, the focus here is on characterizing the 100-m saturated interval from 600 to 700 m amsl that is supported best by selected cutting logs.

Most cutting logs are from either mud- or air-rotary-based drilling methods, so the descriptions are of ground-up sediment. Thus, the descriptions have uncertainty as compared to the descriptions of the retrieved, intact core from the sonic drilling of 19PB. Comparison of logs from three wells drilled adjacent to 19PB (i.e., 19D, 19P, and 191M2) can be used to illustrate one problem in the cutting logs. We know from the 19PB sonic core that the saturated zone alluvium is mostly gravel at this location. In two of the drilling logs (19D and 19P), the logger was able to recognize the cuttings were mostly from gravel. In the 19IM2 log, however, all cuttings were classified as from sand. Thus, we only use logs where cuttings derived from gravel were correctly identified.

4.3. Quantifying proportions and thicknesses of hydrofacies

The cutting logs satisfying our criteria were from Nye County EWDP wells Washburn 1X, 2DB, and 4PB. We used the cutting logs from these wells to develop a facies indicator database using Eq. (1). All original logs were coded by Nye County drillers following the Universal Soil Classification System (USCS) (American Society for Testing and Materials, 1985). We developed the indicator database by coding the USCS lithologic descriptions with integer indicators and sampling the logs at 1.52-m intervals. The lithologic descriptions were coded in three different ways, each toward a different purpose.

The goal of the first analysis was to assess the volume fraction of gravel-dominated sediment at each location. An indicator of "1" was assigned if gravel was present (USCS codes gw, gp, gm, and gc) and "0" if absent. The indicator data were averaged over 20-m intervals to vertically profile the volume fraction of gravel with depth and assess vertical stationarity. The results are shown in Figure 4 (bar plot), together with the number of cutting samples used in obtaining the average volumetric fraction for each interval (the overlaid line plot). We see that over the interval from 620 to 700 m amsl, the sediment of record is predominantly gravel. The results indicate a

high and relatively stationary volume fraction of gravel (or coarser) sediment with depth, consistent with the Ressler, et al. (2000) model. Figure 2 indicates that the locations of these wells are kilometers to the west and east of well 19PB. The consistency between the drilling logs from these wells (i.e., the record of gravel-dominated sediment) and the measured sections on outcrops in Fortymile Wash give broader evidence that the Ressler, et al. (2000) model is representative of the saturated alluvium underlying a significant portion of lower Fortymile Wash.

The second approach to coding the indicator data had the goal of quantifying the amount of clay present ("0" if USCS codes cl, sc, gc, etc.). The logs record an average of 15% occurrence of clay over the interval between 620-m and 700-m elevation. A borehole resistivity log through part of this interval exists for 2DB and is shown in Figure 5. The enhanced electronegativity for intervals in which clay is reported supports the driller's interpretation that clay sediment exists.

Clay intervals may often indicate paleosols. Clay mineral formation would be expected in pedogenesis of sediments of volcanic origin. Furthermore, the proportion of clay in the drilling logs is similar to the proportion of paleosols recorded in the outcrop studies (Ressler, et al., 2000). Also, the drilling records of clay appear more often in intervals associated with sand than with gravel, just as Ressler, et al. (2000) describe paleosols as associated with sand (Ressler, et al., 2000). We use the occurrence of clay minerals in the borehole records as a proxy for direct identification of paleosols when assessing the proportion of the low-permeability hydrofacies in borehole records. Ressler, et al. (2000) did not mention the occurrence of clay within the paleosols (or any other facies) mapped on outcrop, perhaps because fine-clay particles may have been preferentially winnowed away by weathering processes on the outcrop exposures. Even if clay is not strictly associated with paleosols, it seems appropriate to assign clay-rich horizons to a low-permeability hydrofacies category when computing proportions of high- and low-permeability hydrofacies, as noted next from drilling logs.

Finally, following these two exploratory analyses, we adopted an indicator coding for use in Eqs. (2)–(6) above, where all USCS codes had a unique integer-indicator value. The USCS codes gw, gp, sw, sp, and any codes starting with these were grouped into high-permeability hydrofacies. The codes sm, sc, cl, and any codes starting with these

were grouped into low-permeability hydrofacies. We also include 19PB in the analysis, as well as a 90-m lithologic record from another sonic well, 22PC. The results (Figure 6) indicate a high and relatively stationary volume fraction of higher-permeability hydrofacies within the depth interval from 620–700 m amsl. About 0.78 of the alluvium is high-permeability hydrofacies and about 0.22 is low-permeability hydrofacies. This is consistent with the volume fraction of the gravel-dominated, high-permeability facies suggested by Ressler, et al. (2000) in their outcrop study.

Using the indicator database, the vertical mean facies lengths of high- and low-permeability hydrofacies are calculated to be 12.4 m and 3.5 m, respectively. These results are consistent with the values 10 m and 2 m estimated by Ressler, et al. (2000). The analyses using drillers' logs thus further corroborate the appropriateness of the proposed hydrofacies model for the saturated alluvium.

4.4. Assessing lateral dimensions through studies of modern depositional systems

The movement of sediment through gravelly braided rivers is well studied, as is the sedimentary architecture within preserved deposits. These studies have led to useful length-to-width scaling relationships for strata within such deposits. Here we review these studies before showing how they are used in defining lateral transition rates within a Markov chain model.

Bedforms of different scales

Sediment moves in gravely braided rivers within bedforms, defined at different scales. Some of these are shown in Figure 7a. At an intermediate scale, sediment moves in bedforms called unit bars (mostly lobate in shape, as shown). At a larger scale, unit bars assemble and move as a bedform called a compound bar. (The type of compound-bar bedform shown in Figure 7a is a braid bar.) Movement generally occurs only during bank-full flow events. Between such events, the tops of compound bars are exposed, as between active channels in Figure 7a. At a smaller scale, within lobate unit bars, most sediment is moving as bedforms called dunes (not shown in Figure 7a).

Cross sets of different scales, as preserved in bedform deposits

The sediment preserved in a braid-belt deposit has different scales of cross-stratification corresponding to the different scales of bedforms. At an intermediate scale, shown in Figure 7b, are sets of mostly convex-upward strata. The box in Figure 7b-(B) marks one set of these convex-up strata deposited by one unit bar. Though the vast majority of unit-bar deposits have convex-up strata, some concave-up strata occur in scours at the confluence of two channels (Figure 7b-(A) and Figure 3-Facies F3).

At a larger scale, a compound-bar deposit comprises cross sets of many unit-bar deposits. At a still larger scale, a braid belt deposit comprises compound-bar deposits and contains, in minor percentage, concave-upward strata marking where a channel became inactive and was plugged with finer sediment (channel fills). These occur on tops of compound bars [inset, Figure 7b-(B)] or at their margins.

At a smaller scale, within unit bars, are cross sets as shown in the expanded inset of Figure 7b-(B). These cross sets are created by the migration of dune bedforms over a unit bar. One set of trough-cross strata is deposited with movement of an individual dune. Most of the trough-cross strata in a set are concave-up and of sandy gravel. Some are of open framework gravel (OFG). Lunt, et al. (2004) discussed how at this scale, the larger permeability contrast is between strata which are OFG versus non-OFG. Ressler, et al. (2000) describe the common occurrence of OFG strata within the Fortymile Wash unit-bar deposits and, though above the range of permeability they could measure with their methods, suggest that the high permeability of OFG could be a relevant feature to include in transport models.

Summary of scales of cross sets, bedforms, and hydrofacies model

Here we expand the classification of hydrofacies in a hierarchy corresponding to the scales of bedforms and deposits defined previously and to the larger contrasts in permeability. Level I of the hierarchy references smaller scale hydrofacies and level II larger-scale hydrofacies. At level II, the higher-permeability hydrofacies are braid-belt deposits, and the lower-permeability hydrofacies are paleosols (Table 1). A braid-belt

deposit includes mostly compound-bar deposits with minor occurrences of circumscribed channel fills. The compound-bar deposits have two scales of internal cross-stratification created by unit bars and dunes. The pedogenic processes forming paleosols operated on the tops of compound bars because they were subareally exposed for significant periods of time. Thus, in our conceptual model, the paleosols cap the tops of compound-bar deposits, as shown in Figure 8. The regions inside paleosols are not further delineated.

Regions inside the higher-permeability hydrofacies at level II are further delineated at hierarchical level I, according to the larger permeability contrasts. The higher-permeability hydrofacies are the OFG strata created by dune bedforms, and the lower-permeabilty hydrofacies are non-OFG regions (Table 1).

Scaling relationships

Studies of many rivers of different sizes and material types have shown that the ratio of bedform length to bedform width increases with the scale of the bedform (Rubin, et al., 2006). Thus, the geometry of larger scale bedforms is more anisotropic compared to that of smaller-scale bedforms. Furthermore, the ratio of the length to thickness of cross sets scales uniformly with the ratio of the length to height of their formative bedforms. The relationships for the entire range of bedforms for which data are available are shown in Figure 9. The important implication of this relationship is that, for a given bedform type, the aspect ratio of its cross sets is constrained within a certain range. If we know the thickness of the cross set, then we can infer the lateral extent, at least at an order of magnitude level, from knowing the order of magnitude of the aspect ratio on the ordinate in Figure 9. In developing the Markov chain model, as will be seen, we primarily need to specify the typical lateral extent both of a paleosol and an OFG stratum. To infer their average lateral extent, we start by using the scaling relationships in Figure 9 to infer the average lateral extent of compound bars.

Figure 9 shows that a cross set created by a compound bar bedform should have a length-to-thickness ratio on the order of 100. In the Fortymile Wash alluvium, the thickness of a compound bar, as sandwiched between two paleosols, is on the order of

10 m. Thus, the average lateral extent of a compound bar is inferred to be on the order of a kilometer.

The compound bar central to Figure 7a is somewhat longer in the along-stream direction than in the cross-stream direction. Lunt, et al. (2004) quantified the areal aspect ratios of compound bars in an analogous, modern, gravely braided river and found them to be on the order of a factor of two or three. However, with reference to some fixed coordinates, the principal directions of anisotropy from one compound bar to the next vary greatly, corresponding to the nonconsistent orientation of active channels as they migrate within the braid-belt. This makes it difficult to simulate the areal anisotropy in the geometry of compound bar deposits without oversimplifying the orientations of the longer axes. The areal-plane geometric anisotropy is small relative to the vertical-plane anisotropy, and we focus only on the vertical-plane anisotropy in formulating a geostatistical model.

Paleosols cap the tops of compound bars, as illustrated in the sketch in Figure 8. Thus, the average lateral extent of paleosols is taken to be the same as the average lateral extent of a single compound bar on the order of a kilometer. This is consistent with the Ressler, et al. (2000) conception of rather extensive paleosols on the tops of compound bars.

The scaling relationships in Figure 9 are given for cross sets of strata, not an individual stratum. Ressler, et al. (2000) indicated that an OFG stratum has a thickness on the order of several decimeters. This is very similar to the thickness of OFG strata in the analogous modern braid-belt system studied by Lunt, et al. (2004). We use the geometry and proportions of OFG strata quantified by Lunt, et al. (2004) as a guide to the length of OFG strata in Fortymile Wash. Lunt, et al. (2004) found that decimeter-thick OFG strata occur throughout gravely unit bar deposits with lengths on the order of 10 m and an overall volume fraction of about 25% (Figure 10). There is a slightly higher percentage of OFG at the base of unit bars, but we ignore that in our development here. Lunt, et al. (2004) report permeability differences of one to two orders of magnitude between OFG and non-OFG strata.

Up to this point, Figure 9 and some knowledge from analogous deposits were used to infer the average length of hydrofacies defined within the hierarchy. Specifying

the variance in the length and thickness of hydrofacies is also important. Studies in which stratal lengths have been exhaustively measured indicate that lengths and thicknesses tend to have frequency distributions approximately exponential or Gamma (Erlangian) distributed (White and Willis, 2000; Ritzi, 2000; Dai, et al., 2005; Ritzi and Allen-King, 2007). The coefficient of variation in length is typically high, tending toward unity, as is true by definition for an exponential distribution function. This is not surprising when thinking, for example, about the thickness of a lens if measured along all possible vertical lines. The range of measurements typically spans order of magnitude, from minute measurements (e.g., millimeters) at the tip through to measurements of centimeters, decimeters, and possibly meters at the middle. The population of lengths measured among multiple strata has an even larger variance than the subpopulations from one stratum. Based on this knowledge, we assume a coefficient of variation of unity for populations of hydrofacies lengths and thicknesses in the model.

4.5. Defining the transition probabilities and the Markov chain

We first focus on simulating the level II heterogeneity, with the larger-scale higher-and lower-permeability facies (braid-belt deposits and paleosols). Using the univariate statistics obtained in Section 4.3, we can develop the Markov chain models for the two-facies model. The volumetric proportions of the low-permeability and high-permeability facies, p_1 and p_2, were calculated in Section 4.3

$$p_1 = 0.22$$
$$p_2 = 0.78 \tag{17}$$

If the high-permeability facies is chosen as the background category, the transition rate matrix **R** is completely specified by $r_{1,\phi}$, the transition rate of low-permeability facies. In the vertical direction, $r_{1,\mathrm{v}}$ [m^{-1}] is

$$r_{1,\mathrm{v}} = -\frac{1}{\bar{l}_{1,\mathrm{v}}} = -\frac{1}{3.5} \tag{18}$$

where the mean thickness of paleosol was estimated in Section 4.3. To honor probability laws and Eq. (13), the high-permeability background (representing a compound bar deposit) has a mean thickness of (3.5 m)×0.78/0.22, which is 12.4 m. Using the average lateral-length-to-thickness ratio for a compound bar of 100, the average lateral extent of

compound bars is then 1240 m. This defines the average length of a paleosol. Therefore, in the lateral direction

$$r_{1,\mathrm{h}} = -\frac{1}{\bar{l}_{1,\mathrm{h}}} = -\frac{1}{1240} \tag{19}$$

Eqs. (18) and (19) completely define the Markov chain model for facies at level II.

4.6 Simulation using the Markov chain model

Simulating both level I and II unit type distributions at the scale of this work (on the order of km) is computationally challenging because of the high resolution required to represent the thin level I unit types (on the order of cm). We thus focus mainly on simulating level II facies distribution in this section and turn to a stochastic treatment for the effect of level I heterogeneity. The three-dimensional Markov chain model developed in the last subsection is used in sequential indicator simulation followed by simulated quenching to generate geologically plausible realizations of facies distributions, which are conditioned on the final indicator database. The TProGS package developed by Carle (1999) is used in this exercise (see Section 3).

For demonstration purposes, the model domain is chosen to be a 5-km by 5-km by 80-m volume aligned along the main flow direction of the entrenched channel of Fortymile Wash (marked by the thick lined square box on Figure 2). The base elevation of the model is 620 m amsl. The resolution of the model is 50 m in the lateral direction and 1 m in the vertical direction.

Two examples of generated random realizations are shown in Figure 11. The simulation produces a field of paleosol "baffles," each of which represents an occurrence of the low-permeability facies, within a background of the high-permeability facies. The average lateral extent of low-permeability occurrences is 1240 m; however, there is a large variance in extent, over orders of magnitude, with some low-permeability occurrences as limited as ten or a hundred meters across. Thus, the simulation represents the expectation of local discontinuities in the low-permeability paleosols as expressed by Ressler, et al. (2000). The higher-permeability background facies represents the occurrence of compound bar deposits, often with more than one of them in lateral juxtaposition, not laterally separated by the paleosol "caps." Thus, while an individual

compound bar might be 1,240 m across (on average), the higher-permeability background region occurs with a lateral extent of 4,000 m on average (see Figure 9). These are typically on the order of 10 m thick. Overall, the effect is a simulation with high-permeability regions having tortuous connectivity around low-permeability baffles.

Because of the data limitations, flow and transport modeling using one realization can be highly uncertain. The model prediction uncertainty can be addressed in a Monte Carlo simulation manner, through generating an ensemble of realizations of subsurface geology. Representing hierarchical architectures via high-resolution grids is computationally burdensome, if not impractical. Oftentimes, upscaling techniques are employed to transform geologic models into ones that are appropriate for flow and transport models.

4.7. Quantitative analysis of macrodispersion coefficients

The level I unit types (regions of different permeability modes within the braid-belt deposits) were too thin to simulate in the Markov chain analysis. Here we use Eqs. (11)–(14) for an analytical assessment of plume dispersion in level II hydrofacies as a function of conductivity contrast. This analysis is also done within the braid-belt deposits for a comparison of macrodispersion expected at these two different scales.

In our basecase, we use data that are partly derived from Fortymile Wash alluvial deposits. Winterle and Farrell (2002) estimated hydraulic properties for EWDP wells based on Nye County pump tests (Nye County Nuclear Waste Repository Office, 1999; Questa Engineering Corp., 2001) and the core sample analysis performed by Ressler, et al. (2000). After comparing the summary of Winterle and Farrell (2002) with borehole lithologic logs, we estimated the geometric means of paleosol and braid-belt hydrofacies to be 0.2 m/day (i.e., $m_1 = -1.609$) and 4 m/day (i.e., $m_2 = 1.386$), respectively; thus, there is a 20-fold contrast between the two. For reference, the hydraulic conductivity values assigned to the valley-fill alluvial aquifer unit are 4.76 m/day in the DOE site-scale saturated zone flow model (Bechtel SAIC Company, LLC, 2004b) and 3.0 m/day in the NRC site-scale saturated zone flow model (Winterle, 2003). Both models treat the alluvium as a uniform hydraulic unit. The indicator integral scales of paleosols in

vertical and horizontal directions are estimated with Eq. (13) by substituting the mean lengths and volumetric proportion of paleosols into the equation.

The contrast of conductivities between OFG and non-OFG regions at level I typically ranges from 10 to 100 times. For the basecase, we assign 1.23 m/day to non-OFG regions. The mean lengths of the OFG are assumed to be 0.33 m vertically and 10 m laterally, based on our discussion in Section 4.4. The indicator integral scales of OFG can be calculated using Eq. (13) in the same manner as for level I. The data for the basecase are summarized in the last four columns of Table 1. With data in Table 1 and Eq. (9) and (10), we obtain $m_Y = 0.73$, $\sigma_Y^2 = 1.54$ for level II, and $m_Y = 2$, $\sigma_Y^2 = 0.91$ for level I. The mean longitudinal fluid flow velocity U_1 in the alluvial aquifer is estimated to be around 0.01 m/day based on the NRC site-scale flow model (Winterle, 2003).

The sensitivity of macrodispersivities to conductivity contrast at level II is illustrated in Figures 12 and 13. The shapes of the macrodispersivity curves resemble those illustrated in Dagan (1989) for single-modal porous media—at small travel times, the longitudinal macrodispersivity increases linearly with time, whereas at large times, it tends to a asymptotic limit (i.e., the Gaussian regime). For the basecase in which the ratio between geometric means of hydraulic conductivities is 20 (i.e, $\rho = 20$), the asymptotic longitudinal macrodispersivity of around 1500 m is not reached until after 2000 years. Figure 12 shows that D_L increases in proportion to $\ln(\rho)^2$, if all other parameters in Eqs. (11) and (12) are fixed. In comparison, if ρ is fixed and the volumetric proportion is allowed to change, Figure 14 shows that D_L increases with the increase in volumetric proportion of paleosols. This makes sense because more frequent occurrence of the low-permeability paleosol facies creates more baffles and thus more tortuous flow paths at level II.

Figures 15 and 16 demonstrate the sensitivity of level I macrodispersivities to conductivity contrast between the OFG and non-OFG regions within the braid-belt unit type. Because the average scale of unit types is much smaller, it takes less time for the plume to sample all scales at level I, and thus the magnitudes of macrodispersivities are smaller than those of level II. The longitudinal macrodispersivity of the basecase reaches its asymptotic value at around 50 years.

For an alluvial travel distance of 500 m [i.e., the current grid block dimension used in the DOE site-scale saturated zone model (Bechtel SAIC Company, LLC, 2004b)] and the mean fluid velocity assumed in this study (0.01 m/d), the mean travel time is 136 years. At this time, the longitudinal dispersivity predicted by the level II basecase curve in Figure 12 is around 250 m, whereas the level I basecase curve in Figure 15 is around 58 m. Comparing the 500-m distance with the mean lateral lengths listed in Table 1, we can see that 500-m is long enough for a plume to "sample" all level I scales, but not enough to "sample" the average level II scales. As a result, although the dispersivity may have reached the Gaussian regime relative to level I heterogeneity, it continues to grow as the plume starts to encounter more level II heterogeneity. Including the account of level I dispersion does not change the non-Gaussian transport picture at the large scale.

5. Discussion and Summary

The alluvial aquifer Fortymile Wash, Nevada, downstream from the potential Yucca Mountain high-level nuclear waste repository, is expected to be a barrier to transport of radionuclides. A rigorous quantitative approach is taken in this work to assess solute transport behavior by characterizing and modeling the alluvial deposits architecture and subsequently linking the alluvial architecture model to macrodispersion coefficients of solute transport. A hydrofacies model of Fortymile Wash alluvial deposits has been developed on the basis of a combination of geological insight, understanding of depositional processes, outcrop exposure studies, sonic cores and cutting samples, and reported field investigations of similar sedimentary systems.

Cross-stratified deposits, such as those found at Fortymile Wash, can give rise to a hierarchy of permeability modes, corresponding to a hierarchy of facies types across scales. We have employed a two-level hierarchical architecture to describe the Fortymile Wash alluvial deposits, where at the higher level (level II) the system is described by repeated occurrences of paleosol and braid-belt unit types and at the lower level (level I), by the OFG and non-OFG regions within the braid-belt unit type. Markov chain models of transition probabilities are developed from univariate statistics of the sedimentary architecture including volumetric proportions, mean lengths, variance in length, and relative number of occurrences of units. The lateral mean lengths of facies were

constrained by using a scaling relationship developed by Lunt, et al. (2004) based on analysis of bedforms and deposits in several rivers.

Geologically plausible realizations of hydrofacies distributions were generated using sequential indicator simulation with quenching. The results show low-permeability paleosols embedded in the high-permeability braid-belt deposits, creating different fast flow paths and indicating potentially complex resident-time distributions. We focused on simulating facies distributions in the 600–700 m amsl interval, where the volumetric proportions of facies types are approximately stationary and the alluvium mostly is saturated. Our experience shows that the grid dimension in each coordinate direction should be at least one tenth of the mean length in each direction to sufficiently represent spatial variability. This makes simulating geology at large scales a computationally difficult task. Note that in our demonstration, the vertical resolution (1 m) may not sufficiently represent paleosol distribution in the vertical direction, although the resolution for the lateral direction is high enough.

In lieu of pursuing high-resolution numerical simulation, we have used established stochastic theories to link formation heterogeneity at different hierarchical architecture levels with potential solute transport in Fortymile Wash alluvial deposits (Rubin, 1995, 2003; Ritzi, et al., 2004; Dai, et al., 2004). In particular, we estimated macrodispersivities based on three-dimensional Markov chain transition probability models.

The sensitivities of macrodispersivities to hydraulic conductivity contrast were demonstrated. Scale dependency of macrodispersion can affect plume spreading—an increase in longitudinal dispersion shortens the early breakthrough time, whereas an increase in transverse dispersion widens the plume. McKenna, et al. (2003) used high-resolution stochastic continuum models to estimate the transverse and longitudinal macrodispersion that may occur at the sub-gridblock scale within the DOE saturated zone site-scale model, where the dimensions of a gridblock in the site-scale model were defined as 496 by 496 by 48 m at that time. The enhanced permeability fields in the numerical experiment of McKenna, et al. (2003) were generated by superimposing a network of high-permeability features onto a background permeability model, which is generated based on data derived from the volcanic tuff aquifers at Yucca Mountain (thus,

a higher permeability contrast). McKenna, et al. (2003) observed that dispersivities calculated with the enhanced permeability model reached a value of 2380 m after 460 m of travel and appeared to still be rising; in comparison, an expert panel convened by DOE estimated the asymptotic longitudinal dispersivity value to be 100 m after 30 km of travel (Geomatrix Consultants, 1998). The NRC Total-system Performance Assessment code (TPA, Version 5.0.1) assumes the longitudinal dispersivity to be 10 percent of the travel distance in the alluvium, or 100 to 600 m (Farrell, et al., 2005).

In a theoretical study on solute transport in bimodal structures, Dagan and Fiori (2003) concluded that the pre-asymptotic or non-Gaussian regime of solute transport in the presence of very small conductivity zones may last for very long periods of time. Thus, paleosols in the Fortymile Wash alluvium effectively act as solute traps and tend to enhance solute dispersion significantly. For the same reason, solute breakthrough curves will have a long trailing effect. The scale and time dependency of macrodispersivity implies that the fully-mixing condition as implied by the Gaussian transport regime would be unrealistic at the pre-asymptotic stage. The streamline-based methods, which have been used to demonstrate the non-Gaussian nature of the advection-dominated transport in heterogeneous porous media that contains large-scale high- and low-permeability features, would be more appropriate (e.g., Berkowitz and Scher, 2001; Di Donato, et al., 2003).

Only nonreactive cases were considered in this study. The alluvial sedimentary architecture established in this study can be combined with a chemical heterogeneity model [e.g., using the facies-based approach formulated by Allen-King, et al. (1998)]. Existing analyses show the longitudinal dispersivity for sorbing contaminants could be much greater than for nonsorbing solutes, depending on the variability of the sorption coefficient and its correlation with hydraulic conductivity (Gelhar, 1993; Rubin, 2003). The analyses performed in this study provides a detailed quantitative description of facies distributions in Fortymile Wash alluvial aquifer and thus serve as a basic platform based on which uncertainty associated with radionuclide transport can be examined and then propagated through performance assessment models to evaluate the risk.

Acknowledgments

The authors are grateful for our colleagues: P. Bertetti for his constructive comments and D. Waiting for her GIS support. This paper describes work performed by the Center for Nuclear Waste Regulatory Analyses (CNWRA) for the U.S. Nuclear Regulatory Commission (NRC) under Contract No. NRC-02-02-012. The activities reported here were performed on behalf on the NRC Office of Nuclear Material Safety and Safeguards, Division of High-Level Waste Repository Safety. This paper is an independent product of the CNWRA and does not necessarily reflect the view or regulatory position of the NRC.

References

Allen-King, R.M., Halket, R.M., Gaylord, D.R., Robin, M.J.L., 1998. Characterizing the heterogeneity and correlation of perchloroethene sorption and hydraulic conductivity using a facies-based approach. Water Resour. Res., 34(3): 385–396.

American Society for Testing and Materials, 1985. Classification of soils for engineering purposes: Annual book of American Society for Testing and Material Standards (D2487-83). 04.08., 395–408.

Bechtel SAIC Company, LLC, 2004a. Hydrogeologic framework model for the saturated zone site-scale flow and transport model. MDL–NBS–HS–000024. Rev. 00. Las Vegas, Nevada: Bechtel SAIC Company, LLC.

Bechtel SAIC Company, LLC, 2004b. Saturated zone site-scale flow model. MDL–NBS–HS–000011. Rev. 02. Las Vegas, Nevada: Bechtel SAIC Company, LLC.

Bechtel SAIC Company, LLC, 2004c. Site-scale saturated zone transport. MDL–NBS–HS–000010. Rev. 02. Las Vegas, Nevada: Bechtel SAIC Company, LLC.

Bechtel SAIC Company, LLC, 2004d. Saturated zone flow and transport model abstraction. MDL–NBS–HS–000021. Rev. 02. Las Vegas, Nevada: Bechtel SAIC Company, LLC.

Berkowitz, B., Scher, H., 2001. The role of probabilistic approaches to transport theory in heterogeneous media. Transport in Porous Media, 42(1–2): 241–263.

Carle, S.F., Fogg, G.E., 1996. Transition probability-based indicator geostatistics. Math. Geol., 28(4): 453–476.

Carle, S.F., Fogg, G.E., 1997. Modeling spatial variability with one- and multi-dimensional continuous Markov chains. Math. Geol. 29(7): 891–918.

Carle, S.F., 1999. T-PROGS: Transitional Probability Geostatistical Software. User's Guide. Davis, California: University of California.

Carle, S.F., LaBolle, E.M., Weissmann, G.S., VanBrocklin, D., Fogg, G.E., 1998. Conditional simulation of hydrofacies architecture: A transition probability/Markov approach—Vol. 1: Environmental Geology. Hydrogeologic Models of Sedimentary Aquifers, SEPM Concepts in Hydrogeology. G.S. Fraser and J.M. Davis, eds. Tulsa, Oklahoma: Society for Sediment Geology, 147–170.

Collinson, J.D., 1996. Alluvial environments, in Sedimentary Environments and Facies, 3rd ed. Edited by H.G. Reading, pp. 37–82. New York, New York: Elsevier.

Dagan, G., 1989. Flow and Transport in Porous Formations. New York, New York: Springer-Verlag.

Dagan, G., Fiori, A., 2003. Time-dependent transport in heterogeneous formations of bimodal structures: 1. The model. Water Resour. Res., 39(5), doi:10.1029/2002WR001396.

Dai, Z., R.W. Ritzi Jr., C. Huang, Y. Rubin, and D.F. Dominic (2004), Transport in heterogeneous sediments with multimodal conductivity and hierarchical organization across scales, J. Hydrol., 294(1–3), 68–86.

Dai, Z., Ritzi, R.W., Dominic, D.F., 2005. Improving permeability semivariograms with transition probability models of hierarchical sedimentary architecture derived from outcrop-analog studies. Water Resour. Res. 41, W07032, doi:10.1029/2004WR002515.

de Marsily, G., Delay, F., Gonçalvès, J., Renard, P., Teles, V., Violette, S., 2005. Dealing with Spatial Heterogeneity. Hydrogeol. J. 13: 161–183.

Desbarats, A.J., 1990. Macrodispersion in sand-shale sequences. Water Resour. Res., 26(1): 153–163.

Di Donato, G., Obi, E.-O., Blunt, M. J., 2003. Anomalous transport in heterogeneous media demonstrated by streamline-based simulation. Geophys. Res. Lett., 30(12): 1608, doi:10.1029/2003GL017196.

Farmer, C.L., 2002. Upscaling: A Review. Int. J. Numer. Meth. Fl., 40: 63–78.

Farrell, D.A., Rankin, V., Buseman-Williams, A., 2005. Development and application of a model to simulate saturated zone transport from the location of the proposed repository footprint at Yucca Mountain. San Antonio, Texas: CNWRA.

Gelhar, L.W., 1993. Stochastic Subsurface Hydrology. Englewood Cliffs, New Jersey: Prentice Hall.

Geomatrix Consultants, 1998. Saturated Zone Flow and Transport Expert Elicitation Project. Deliverable Number SL5X4AM3. Las Vegas, Nevada: CRWMS M&O.

Kamann, P.R., Ritzi, R.W., Dominic, D.F., Dai, Z. Porosity and permeability in sediment mixtures. Ground Water. In press.

Koltermann, C., Gorelick, S.M., 1996. Heterogeneity in sedimentary deposits: A review of structure-imitating, process-imitating, and descriptive approaches. Water Resour. Res., 32(9): 2617–2657.

Lin, C., Harbaugh, J.W., 1984. Graphic Display of Two- And Three-Dimensional Markov Computer Models in Geology. 180 pp. New York, New York: Van Nostrand Reinhold.

Livesey, J.R., Bennett, S., Ashworth, P.J., Best, J.L., 1998. Flow structure, sediment transport and bedform dynamics for a bimodal sediment mixture. In: gravel-Bed Rivers in the Environment (Eds P.C. Klingeman, R.L. Beschta, P.D. Koman and J.B. Bradley), pp. 149-176. Water Resources Publications, Colorado.

Lu, Z., Zhang, D., 2002. On stochastic modeling of flow in multimodal heterogeneous formations. Water Resour. Res., 38(10), doi:10.1029/2001WR001026.

Lundstrom, S.C., Paces, J.B., Mahan, S.A., 1998. Late Quaternary history of Fortymile Wash in the area near the H-Road crossing. Quaternary Geology of the Yucca Mountain area, southern Nevada: Field trip guide. Friends of Pleistocene, Pacific Cell. 63–76.

Lundstrom, S.C., Warren, R.G., 1994. Late Cenozoic evolution of Fortymile Wash: Major change in drainage pattern in the Yucca Mountain, Nevada region during late Miocene volcanism. Proceedings of the 5th Annual International Conference on High-Level Radioactive Waste Management, Las Vegas, Nevada, May 22–26, 2121–2130.

Lunt, I.A., Bridge, J.S., Tye. R.S., 2004. A quantitative, three-dimensional depositional model of gravely-braided rivers. Sedimentology, Vol. 51. doi:10.1111/j.1365-3091.2004.00627.x.

McKenna, S.A., Walker, D.D., Arnold, B., 2003. Modeling dispersion in three-dimensional heterogeneous fractured media at Yucca Mountain. J. Contam. Hydrol., 62–63: 577–594.

Miall, A.D., 1996. The Geology of Fluvial Deposits. New York, New York: Springer.

Nye County Nuclear Waste Repository Project Office, 2007. http://www.nyecounty.com/ewdpmain.htm. Accessed February 10, 2007.

Nye County Nuclear Waste Repository Project Office, 2005. Nye County Early Warning Drilling Program Phase IV Drilling Report. Nye County, Nevada: Nye County Nuclear Waste Repository Project Office.

Nye County Nuclear Waste Repository Project Office, 1999. Phase I, FY1999 data package for Early Warning Drilling Program. Nye County, Nevada: Nye County Nuclear Waste Repository Project Office.

NRC, 2005. NUREG–1762, Integrated Issue Resolution Status Report. Rev. 1. Washington, DC: NRC. April.

Potter, C.J., Dickerson, R.P., Sweetkind, D.S., Drake, R.M., Taylor, E.M., Fridrich, C.J, San Juan, C.A., Day, W.C. 2002. Geologic map of the Yucca Mountain Region, Nye County, Nevada. Pamphlet accompanying U.S. Geological Survey Investigation Series I–2755.

Proce, C.J., Ritzi, R.W., Dominic, D.F., Dai, Z., 2004. Modeling multiscale heterogeneity and aquifer interconnectivity. Ground Water, 42(5): 658–670.

Questa Engineering Corp., 2001. Analysis of pump-spinner test and 48-hour pump test in Well NC-EWDP-19D, near Yucca Mountain, Nevada. NWRPO–2001–03. Nye County, Nevada: Nye County Nuclear Waste Repository Project Office.

Ressler, T.R., Stamatakos, J.A., Ridgeway, K.D., Winterle, J., 2000. Preliminary hydrostratigraphy of the valley-fill aquifer in Fortymile Wash and the Amargosa Desert. San Antonio, Texas: CNWRA.

Ritzi, R.W., 2000. Behavior of indicator variograms and transition probabilities in relation to the variance in lengths of hydrofacies. Water Resour. Res., 36(11): 3375–3381.

Ritzi, R.W., Dai, Z., Dominic, D.F., Rubin, Y., 2004. Spatial correlation of permeability in cross-stratified sediment with hierarchical architecture. Water Resour. Res., 40, W03513, doi:10.1029/2003WR002420.

Ritzi, R.W., Allen-King, R.M., 2007. Why did Sudicky [1986] find an exponential-like spatial correlation structure for hydraulic conductivity at the Borden research site. Water Resour. Res., 43, W01406, doi:10.1029/2006WR004935.

Rubin, Y., 1995. Flow and transport in bimodal heterogeneous formation. Water Resour. Res., 31(10): 2461–2468.

Rubin, Y., 2003. Applied Stochastic Hydrogeology. 416 pp. New York, New York: Oxford Press.

Rubin, Y., Lunt, I.A., Bridge, J.S., 2006. Spatial variability in river sediments and its link with river channel geometry. Water Resour. Res., 42, W06D16, doi:10.1029/2005WR004853. 2006.

Weissmann, G.S., Fogg, G.E., 1999. Multiple-scale alluvial fan heterogeneity modeled with transition probability geostatistics in a sequence stratigraphic framework. J. Hydrol., 226: 45–48.

White, C.D., Willis, B.J., 2000. A method to estimate length distributions from outcrop data. Math. Geol., 32(4): 389–419.

Winterle, J.R., Farrell, D.A., 2002. Hydrogeologic properties of the alluvial basic beneath Fortymile wash and northern Amargosa Valley, southern Nevada. San Antonio, Texas: CNWRA.

Winterle, J.R., 2003. Evaluation of alternative concepts for saturated zone flow: Effects of recharge and water table rise on flow paths and travel times at Yucca Mountain. San Antonio, Texas: CNWRA.

Table 1. Fortymile Wash alluvial deposits hierarchical architecture and the corresponding data

Level	Direction	Unit Type	Proportion	Mean Length, m	λ_I, m	$\langle Y_i \rangle$
II	Vertical	Paleosol	0.22	3.5	2.73	-1.609
		Braid-belt	0.78	12.4	2.73	1.386
	Horizontal	Paleosol	0.22	1240	968	-1.609
		Braid-belt	0.78	4400	968	1.386
I	Vertical	OFG	0.22	0.33	0.26	2.51
		Non-OFG	0.78	1.17	0.26	0.21
	Horizontal	OFG	0.22	10	7.8	2.51
		Non-OFG	0.78	35.5	7.8	0.21

Figure Captions

Figure 1. Satellite image of Yucca Mountain and its surrounding area. Fortymile Wash and its entrenched channel are labeled on the image. Map coordinates are Universal Transverse Mercator, Zone 11, North American Datum of 1983, meters.

Figure 2. Locations of the five outcrop exposures studied by Ressler et al. (2000) (small filled circles in orange), and Nye County EWDP wells drilled in Fortymile Wash basin. The wells used in the final indicator database are marked with large open circles. The square box delimits the areal extent of the simulation model (see Section 4.6).

Figure 3. Left top: Picture of a representative outcrop exposure studied by Ressler, et al. (2000). Left bottom: Facies distribution modeled by Ressler, et al. (2000). Right: Facies modeled by Ressler, et al. are categorized into the paleosol and braid-belt facies comprising level II of the current hydrofacies model.

Figure 4. The volume proportion of gravels over depth. The values are averaged over every 20 m in the 600–700 m amsl (bar plot). The top axis shows the number of samples used to calculate the average volume fraction for each internal (line plot).

Figure 5. Comparison between EWDP 2DB borehole resistivity (line) and indicator codings (squares). The plot shows that the codings based on drillers' logs capture the clay distribution in 2DB well and are in good agreement with the borehole resistivity measurements. The interval is saturated, and the resistivity lows are assumed to be mainly caused by the presence of clay content.

Figure 6. Volumetric proportions of high-permeability (the left-hand-side group on the bar plot) and low-permeability (the right-hand-side group on the bar plot) hydrofacies. The bar plot shows relatively stationary volume proportion over the 620–700 m amsl interval. The top axis shows the number of observations used in calculating the volume proportion over each 10-m interval.

Figure 7. A braided fluvial system studied by Lunt, et al. (2004). (a). Depositional model of gravelly braided river deposits. Map showing idealized channels, compound bars, and unit bars in active and abandoned channels. (b). A hierarchy of stratal unit types. Cross-sections showing large-scale inclined strata from deposits in the active part of the channel belt. Thick lines represent bases of compound sets, medium lines represent bases of large-scale sets, and thin lines represent large-scale strata. Adapted from Figure 24a&b of Lunt, et al. (2004).

Figure 8. Compound bar deposits that consist of many embedded single compound bars. The average lateral extent of a single compound bar is on the order of 1000 m. The paleosols cap the tops of the compound bars and thus have the same average lateral extent as that of a single compound bar.

Figure 9. Length-to-height ratio of bedforms plotted against strataset length-to-thickness ratio. The average length-to-thickness ratio of compound bar deposits is around 228. (Figure 5 of Rubin, et al., 2006).

Figure 10. Distribution of sediment types within normalized thickness of simple large-scale sets. The overall volume fraction of open-framework gravels is about 25%. Adapted from Figure 19 of Lunt, et al. (2004).

Figure 11. Two realizations of hydrofacies distributions produced by conditional sequential indicator simulation followed by simulated quenching (TProGS, Carle, 1999) using the three-dimensional Markov chain model developed for alluvial deposits of Fortymile Wash.

Figure 12. Level II longitudinal macrodispersivity as a function of travel time, *t*, and ratio of geometric mean conductivity, ρ, between braid-belt and paleosol hydrofacies.

Figure 13. Level II transverse macrodispersivity as a function of travel time, *t*, and ratio of geometric mean conductivity, ρ, between braid-belt and paleosol hydrofacies.

Figure 14. The product $\sigma_Y^2 \lambda_I$ as a function of the volumetric proportion of paleosols. The *y*-axis is normalized by the basecase values $\sigma_{Y0}^2 \lambda_{I0}$

Figure 15. Level I longitudinal macrodispersivity as a function of travel time, *t,* and ratio of geometric mean conductivity*,* ρ, between OFG (open-framework gravels) and non-OFG regions within the braid-belt facies.

Figure 16. Level I transverse macrodispersivity as a function of travel time, *t*, and ratio of geometric mean conductivity, ρ, between OFG and non-OFG regions within the braid-belt facies.

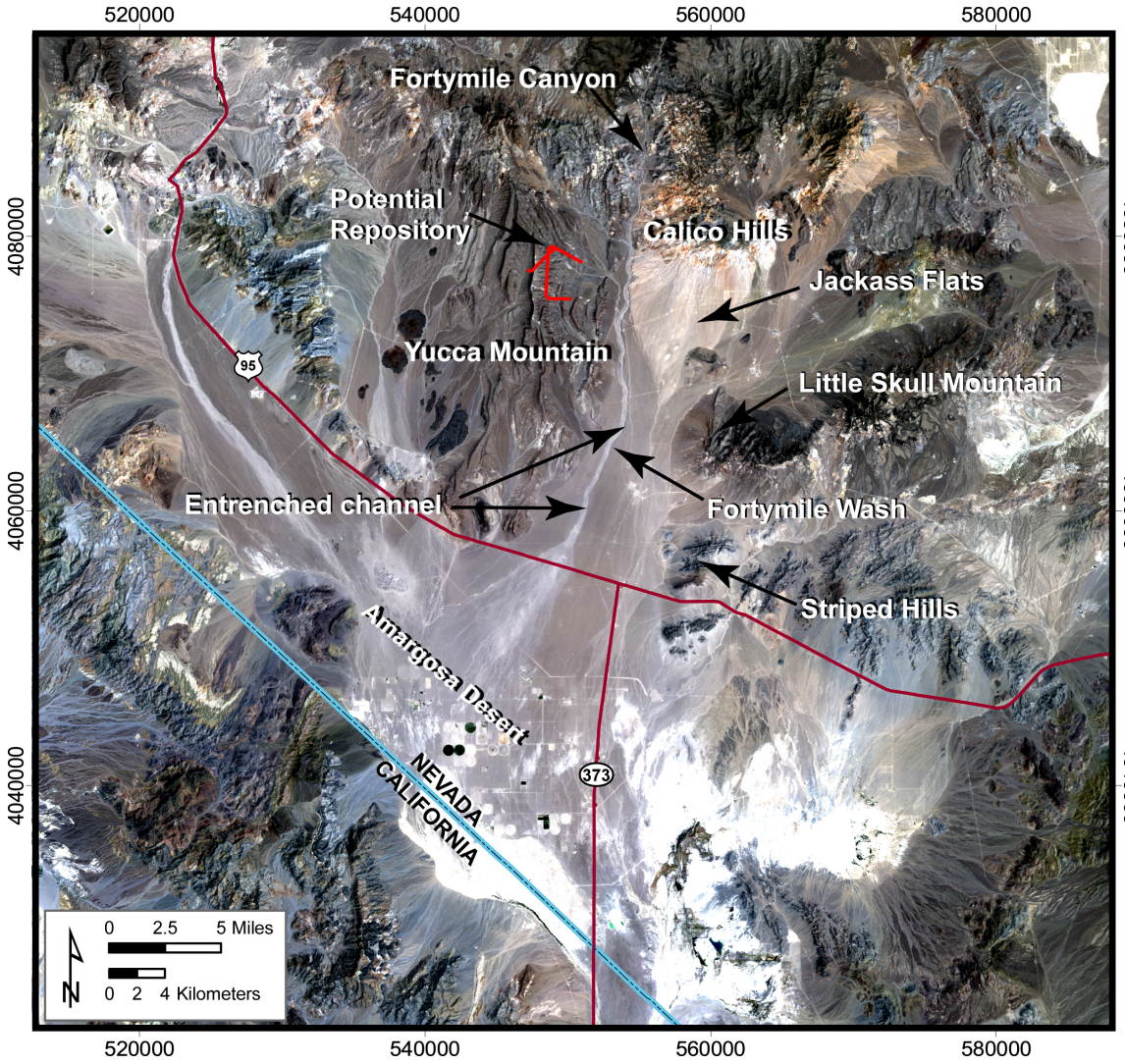

Figure 1. Satellite image of Yucca Mountain and its surrounding area. Fortymile Wash and its entrenched channel are labeled on the image. Map coordinates are Universal Transverse Mercator, Zone 11, North American Datum of 1983, meters.

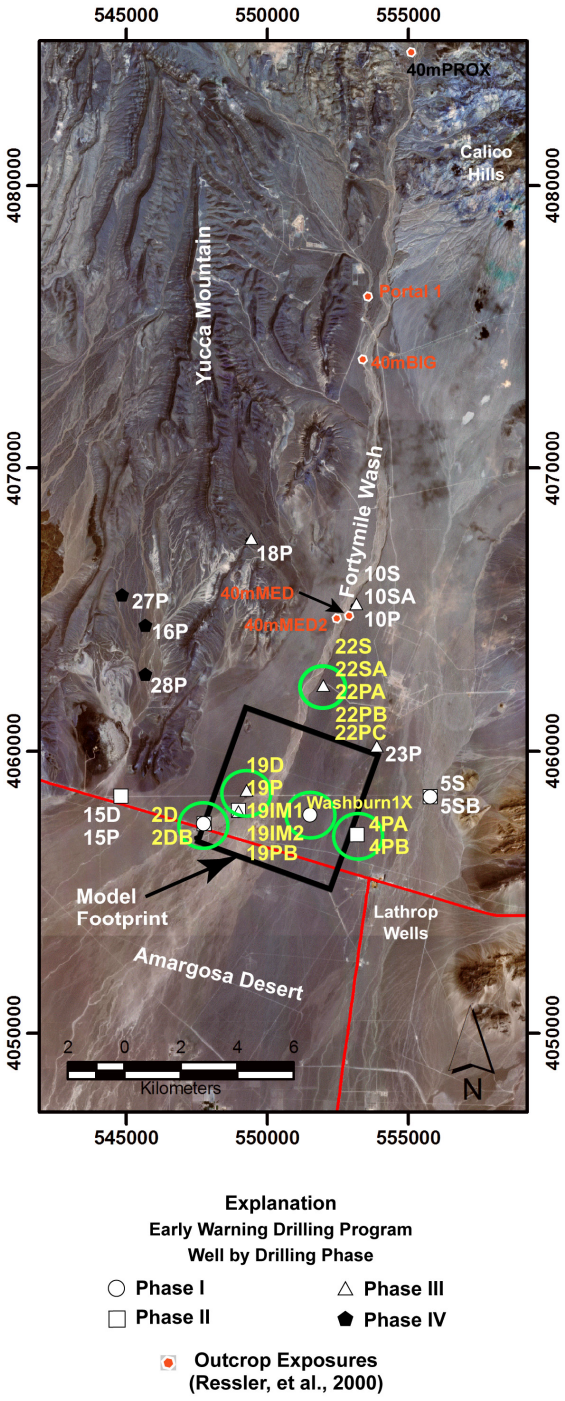

Figure 2. Locations of the five outcrop exposures studied by Ressler et al. (2000) (small filled circles in orange), and Nye County EWDP wells drilled in Fortymile Wash basin. The wells used in the final indicator database are marked with large open circles. The square box delimits the areal extent of the simulation model (see Section 4.6).

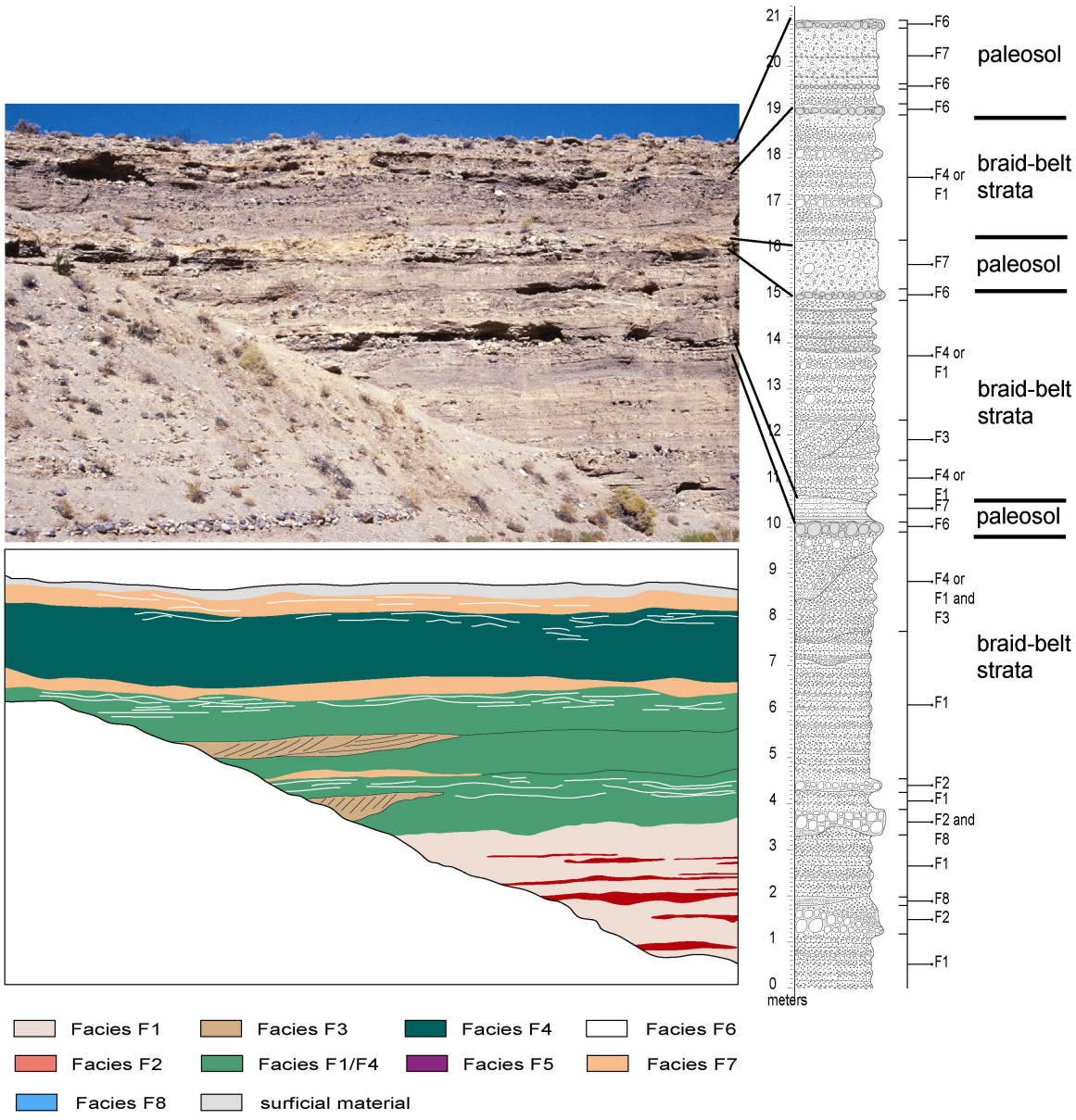

Figure 3. Left top: Picture of a representative outcrop exposure studied by Ressler, et al. (2000). Left bottom: Facies distribution modeled by Ressler, et al. (2000). Right: Facies modeled by Ressler, et al. are categorized into the paleosol and braid-belt facies comprising level II of the current hydrofacies model.

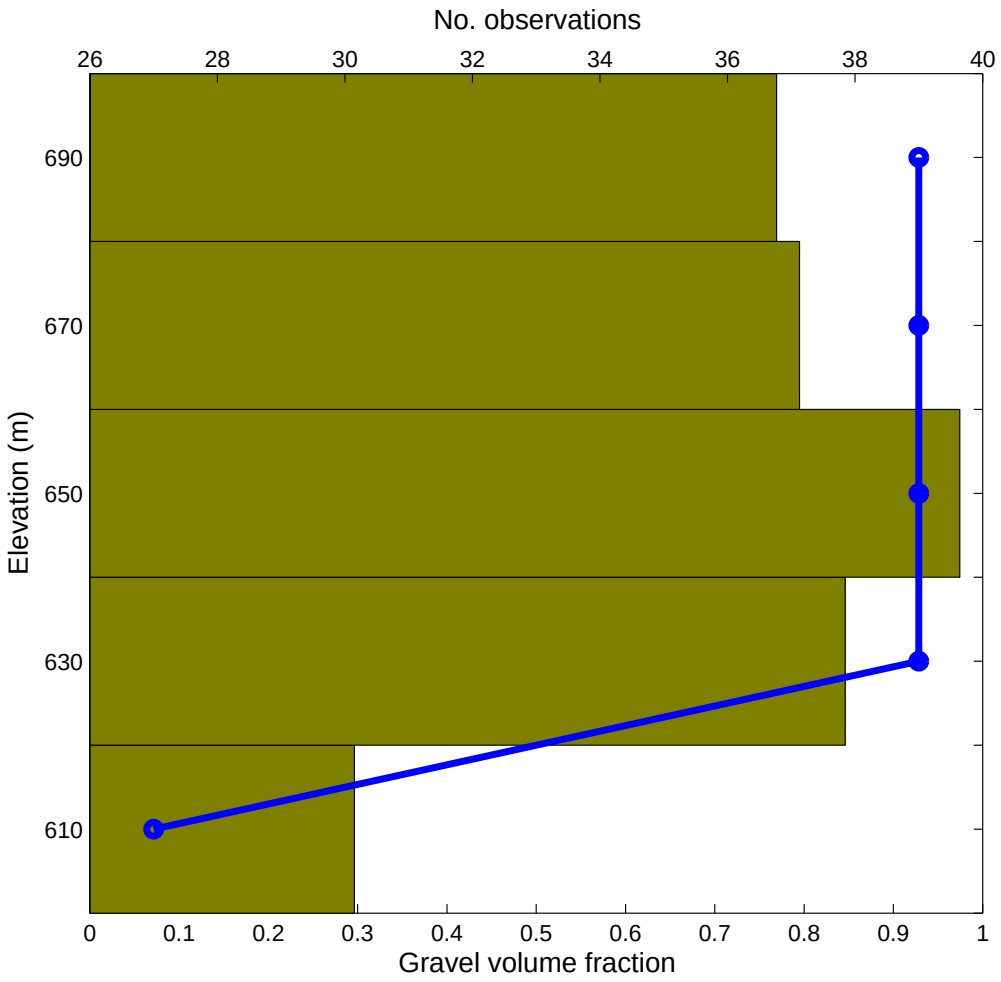

Figure 4. The volume proportion of gravels over depth. The values are averaged over every 20 m in the 600–700 m amsl (bar plot). The top axis shows the number of samples used to calculate the average volume fraction for each internal (line plot).

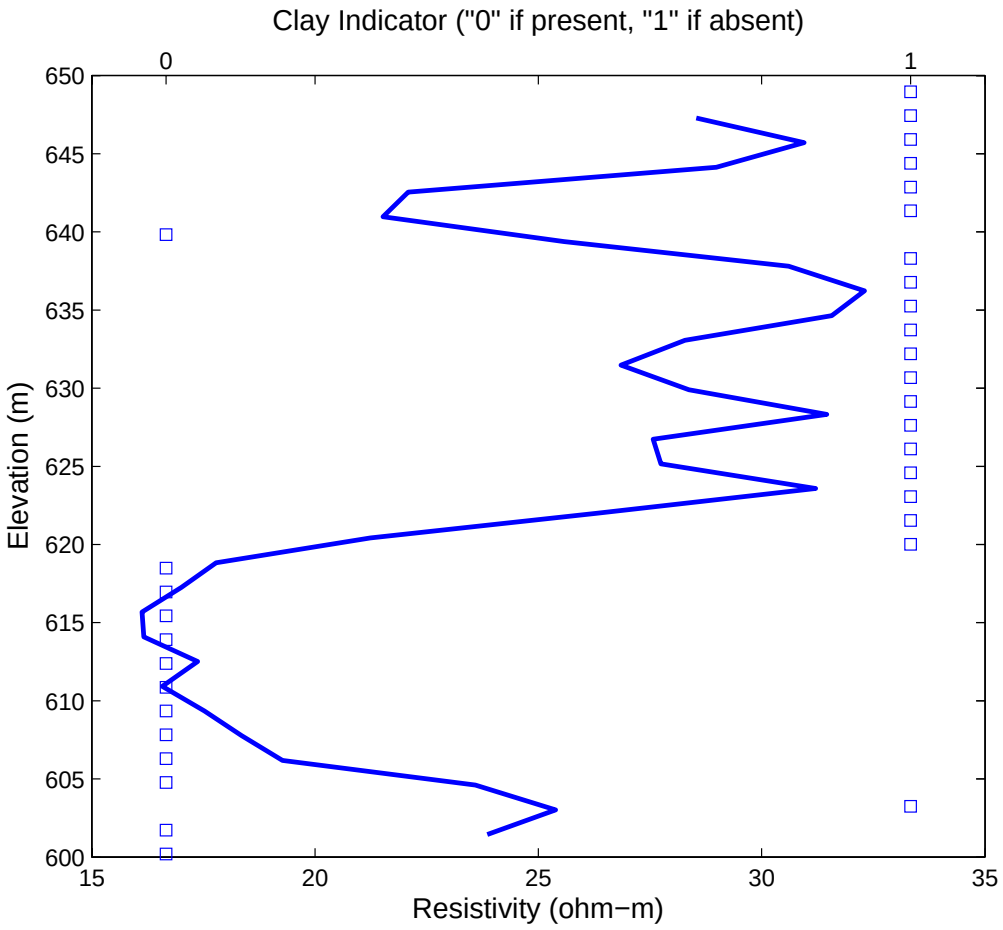

Figure 5. Comparison between EWDP 2DB borehole resistivity (line) and indicator codings (squares). The plot shows that the codings based on driller's logs capture the clay distribution in 2DB well and are in good agreement with the borehole resistivity measurements. The interval is saturated and the resistivity lows are assumed to be mainly caused by the presence of clay content.

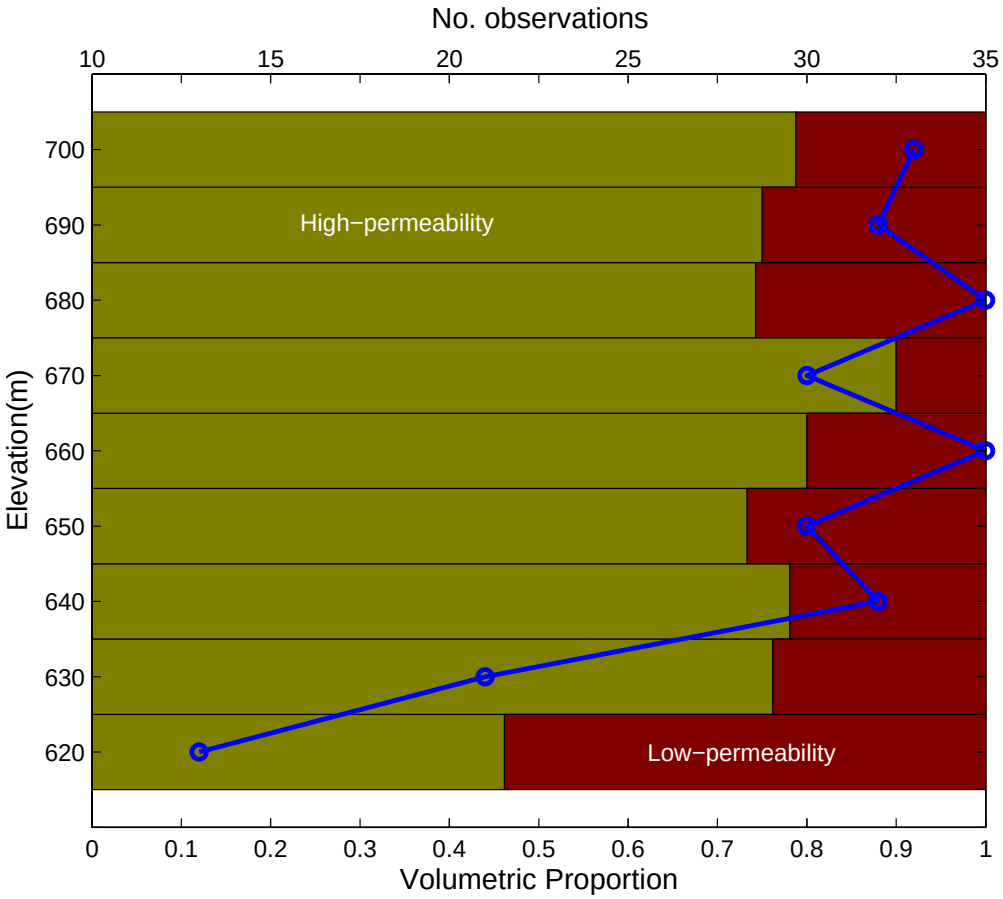

Figure 6. Volumetric proportions of high-permeability (the left-hand-side group on the bar plot) and low-permeability (the right-hand-side group on the bar plot) hydrofacies. The bar plot shows relatively stationary volume proportion over the 620–700 m amsl interval. The top axis shows the number of observations used in calculating the volume proportion over each 10–m interval.

Figure 7(a)

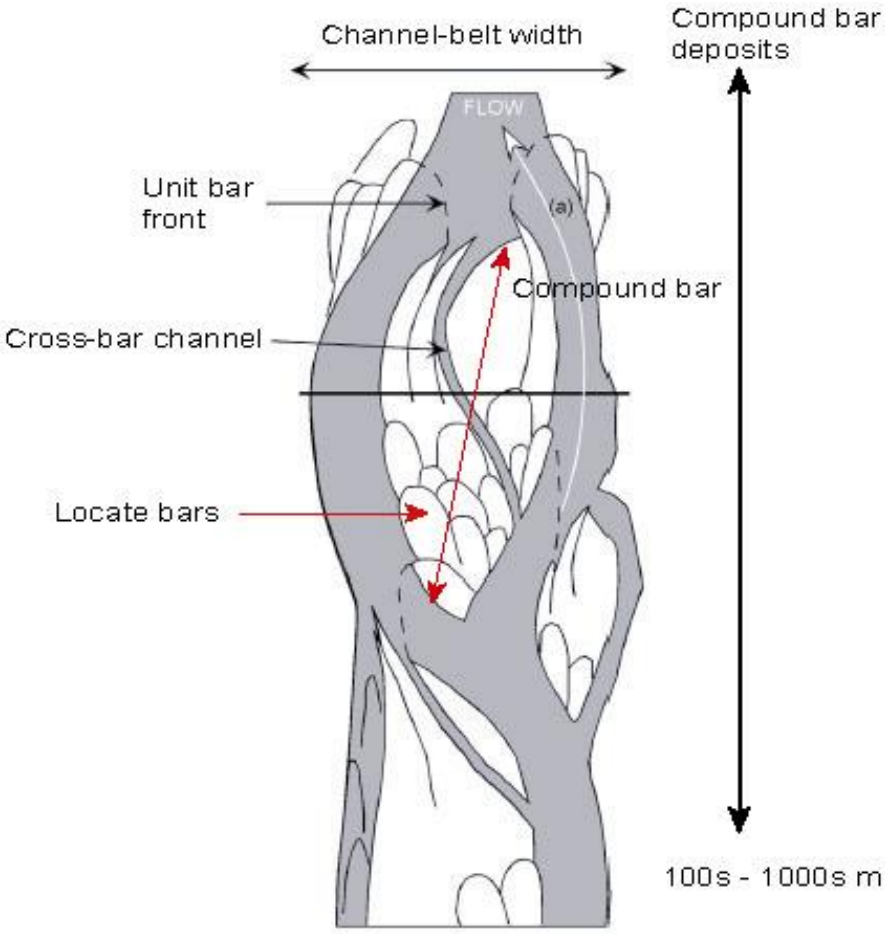
Channel-belt width
Compound bar deposits
FLOW
Unit bar front
(a)
Compound bar
Cross-bar channel
Locate bars
100s - 1000s m

Figure 7(b)

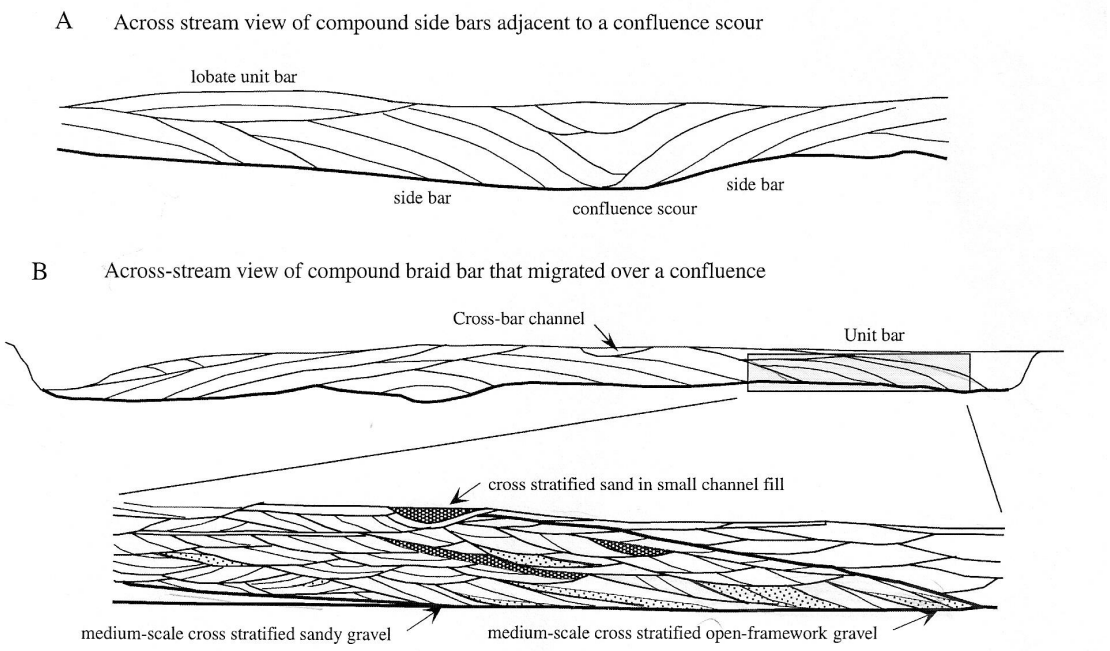

Figure 7. A braided fluvial system studied by Lunt, et al. (2004). (a). Depositional model of gravelly braided river deposits. Map showing idealized channels, compound bars, and unit bars in active and abandoned channels. (b). A hierarchy of stratal unit types. Cross-sections showing large-scale inclined strata from deposits in the active part of the channel belt. Thick lines represent bases of compound sets, medium lines represent bases of large-scale sets, and thin lines represent large-scale strata. Adapted from Figure 24a&b of Lunt, et al. (2004).

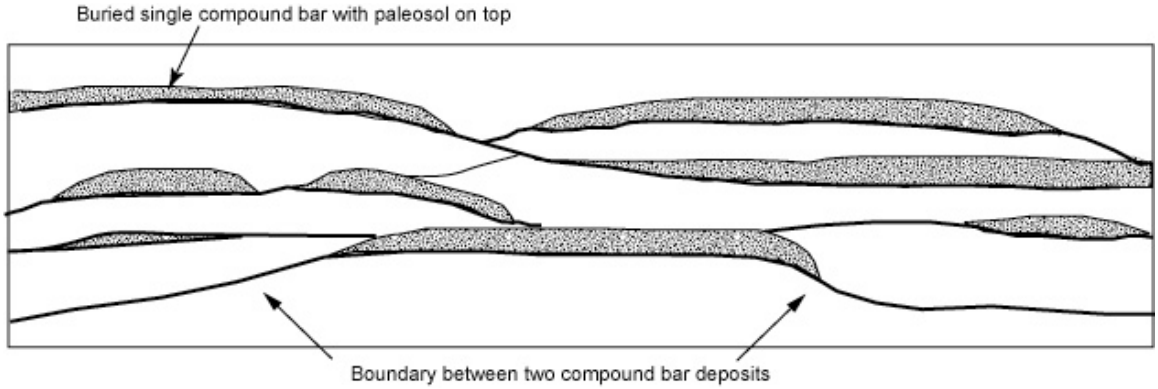

Figure 8. Compound bar deposits consisting of many embedded single compound bars. The average lateral extent of a single compound bar is on the order of 1000 m. The paleosols cap the tops of compound bar and thus, having the same average lateral extent as that of a single compound bar.

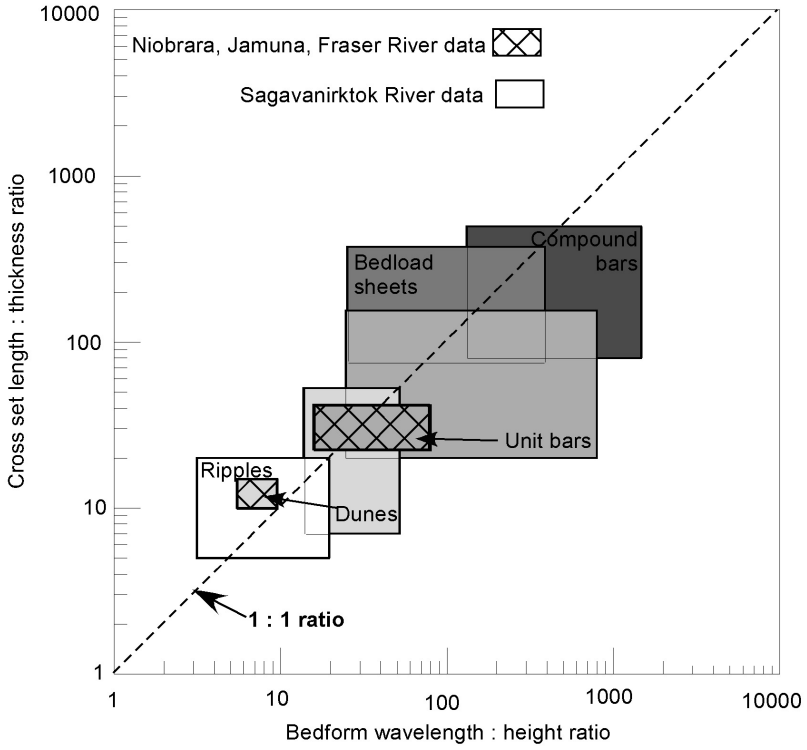

Figure 9. Length-to-height ratio of bedforms plotted against strataset length-to-thickness ratio. The average length-to-thickness ratio of compound bar deposits is around 228. (Figure 5 of Rubin, et al., 2006).

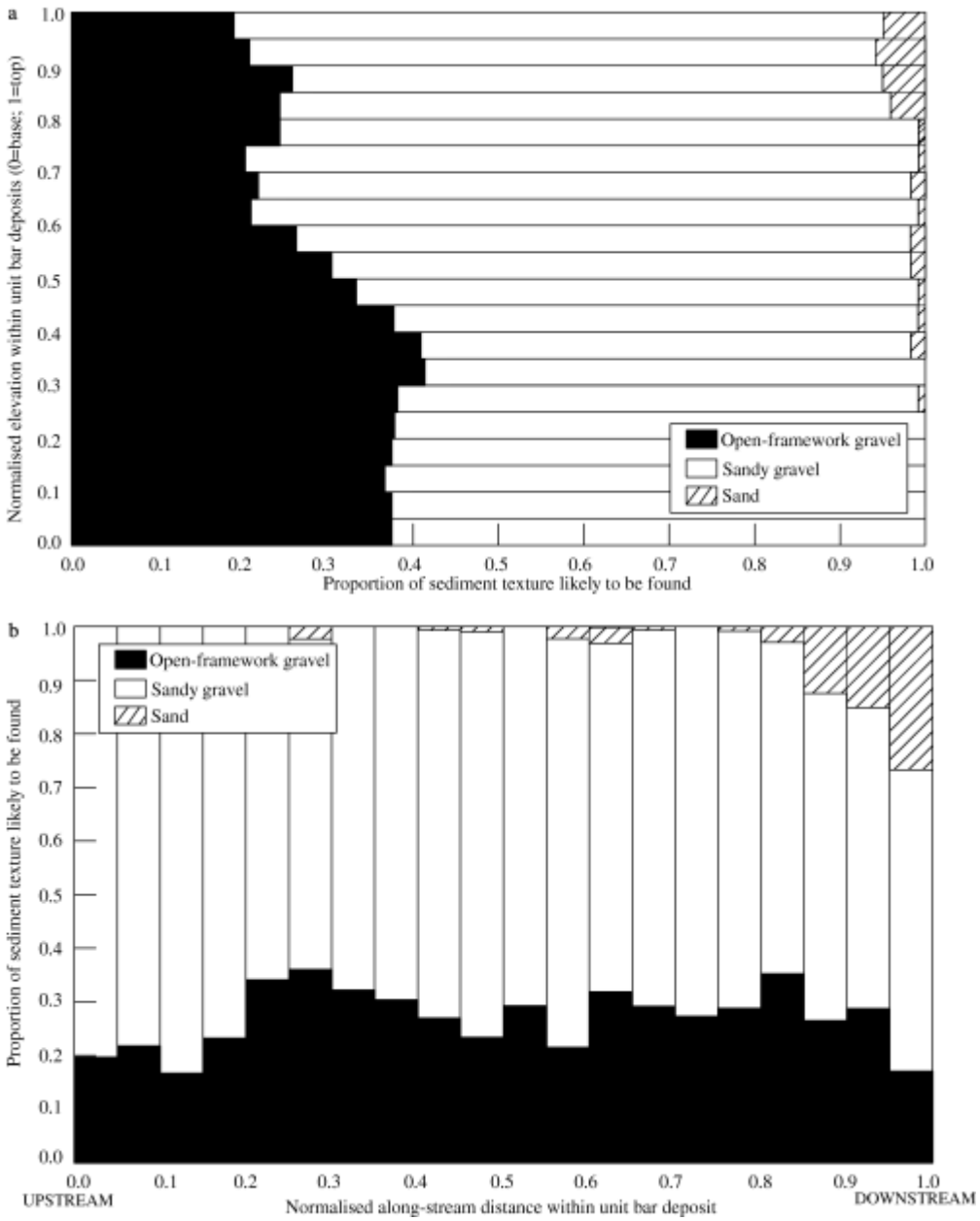

Figure 10. (a). Distribution of sediment types within normalized thickness of simple large-scale sets. 0 and 1 are the base and top the unit-bar deposit respectively. (b). Distribution of sediment types along the normalized length of untruncated unit-bar deposits. 0 is upstream and 1 is downstream. The overall volume fraction of open-framework gravels is about 25% (Figure 19 of Lunt, et al., 2004).

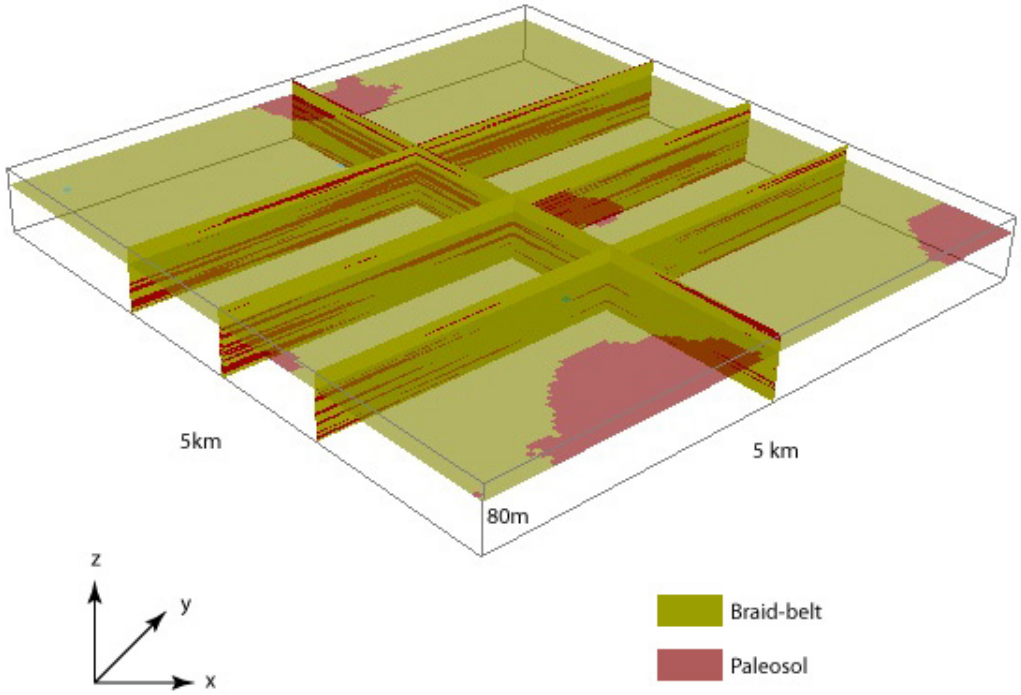

Figure 11. Two realizations of hydrofacies distributions produced by conditional sequential indicator simulation followed by simulated quenching (TProGS, Carle, 1999) using the three-dimensional Markov chain model developed for alluvial deposits of Fortymile Wash.

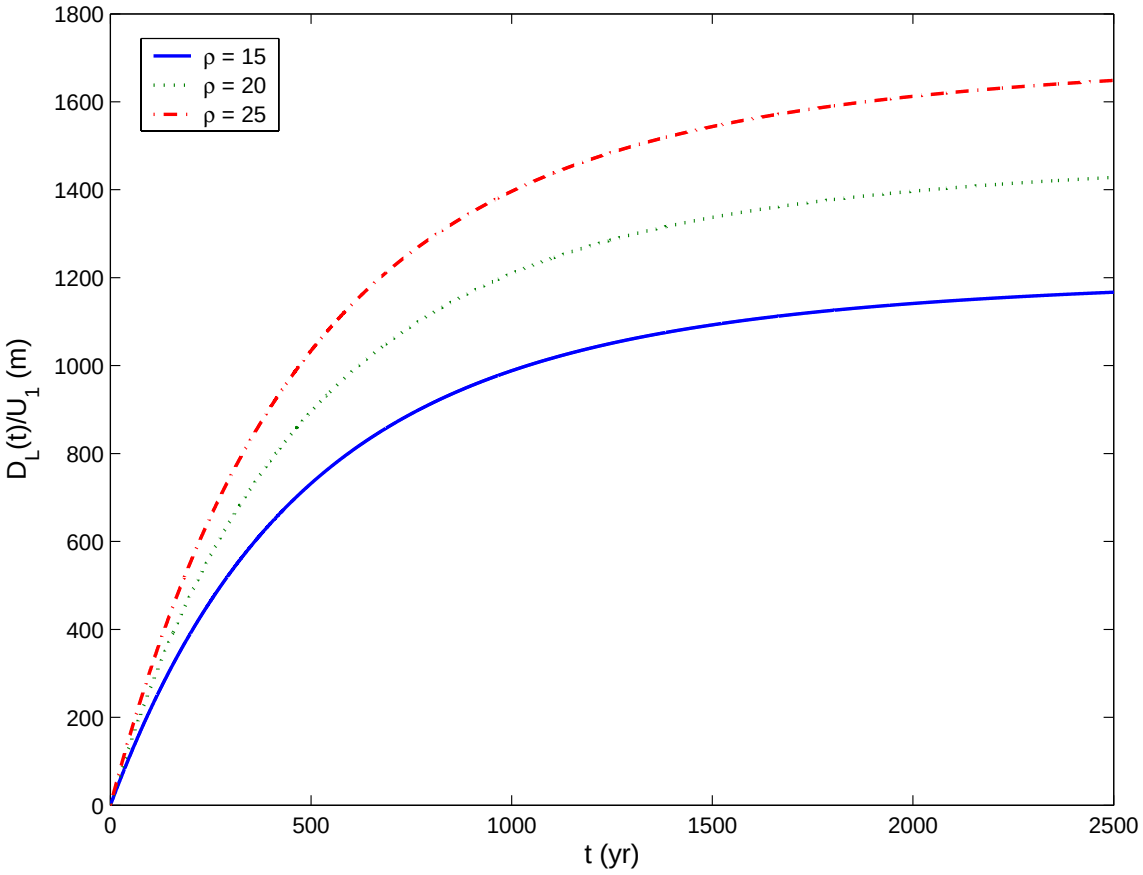

Figure 12. Level II longitudinal macrodispersitivity as a function of travel time, *t*, and ratio of geometric mean conductivity, ρ, between braid-belt and paleosol stratal unit types.

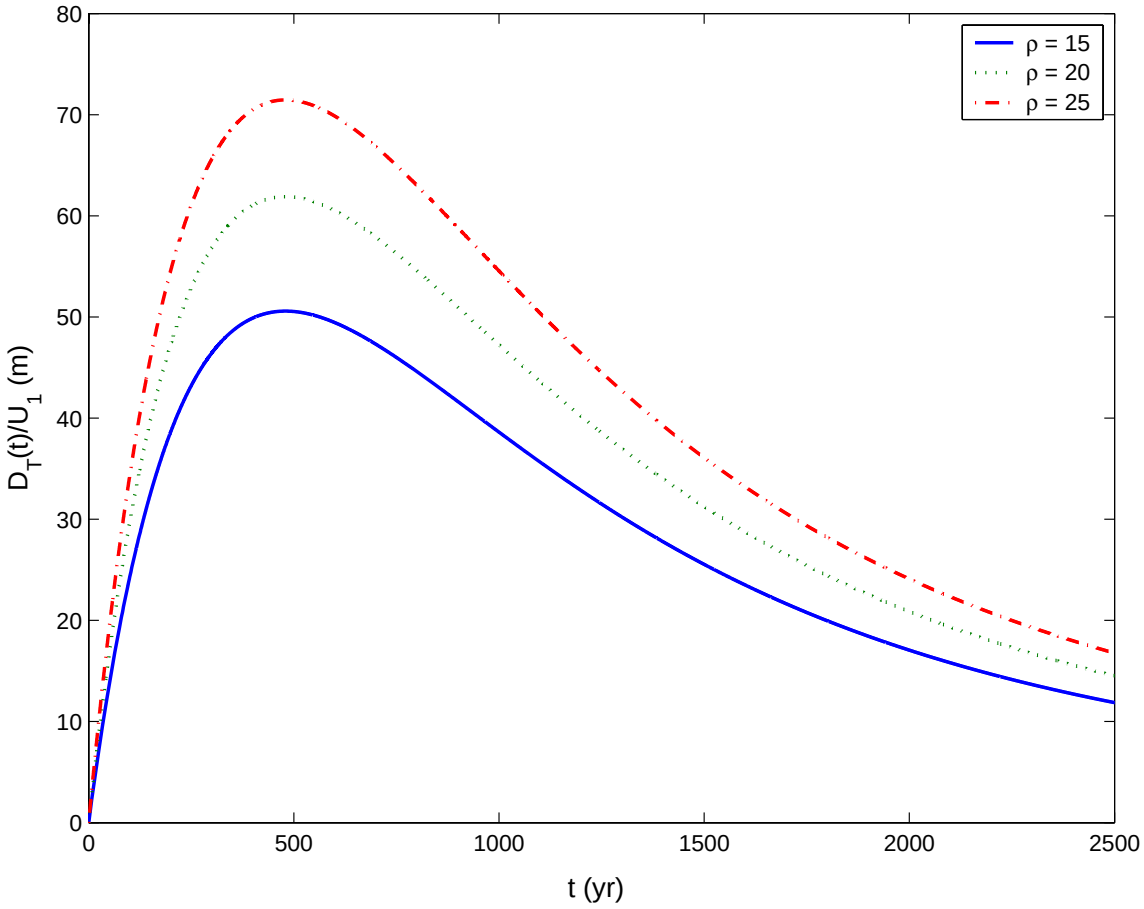

Figure 13. Level II transverse macrodispersitivity as a function of travel time, *t*, and ratio of geometric mean conductivity, ρ, between braid-belt and paleosol stratal unit types.

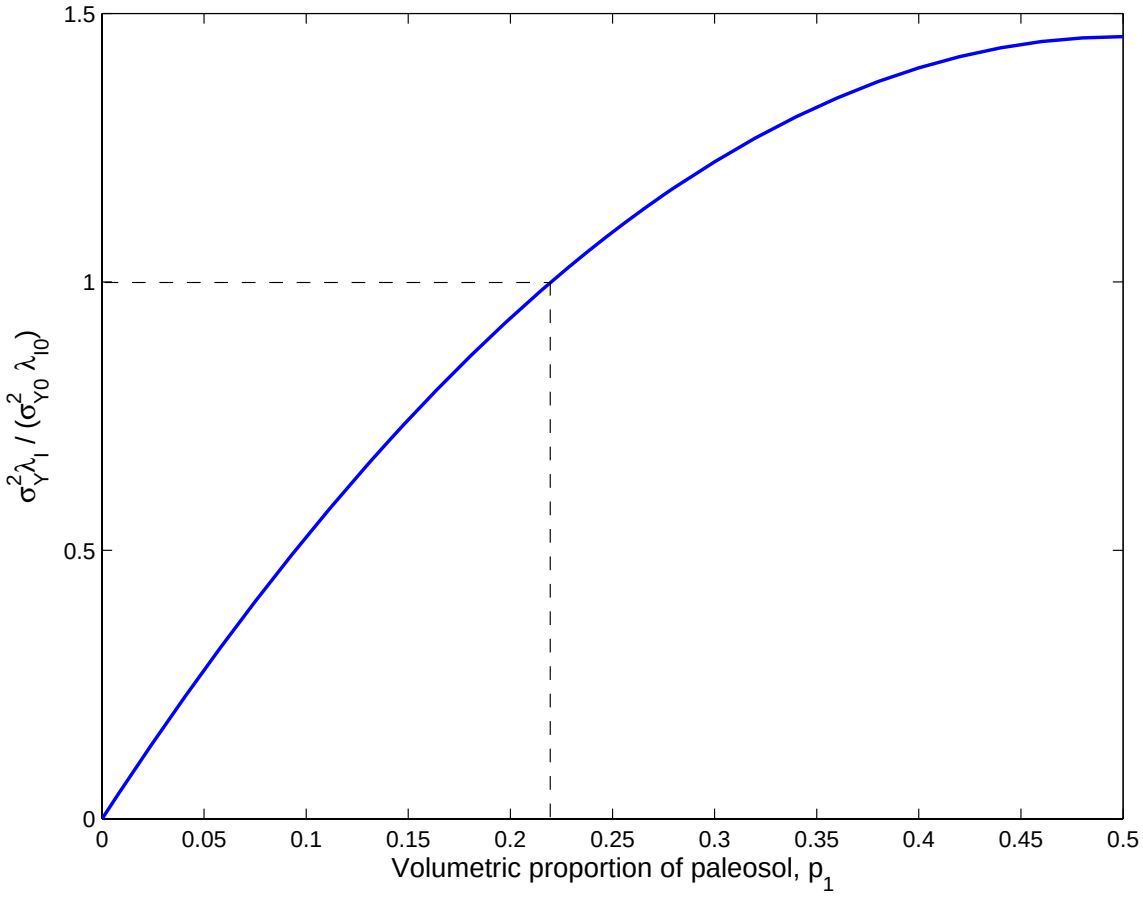

Figure 14. The product $\sigma_Y^2 \lambda_I$ as a function of the volumetric proportion of paleosols. The *y*-axis is normalized by the base case values $\sigma_{Y0}^2 \lambda_{I0}$

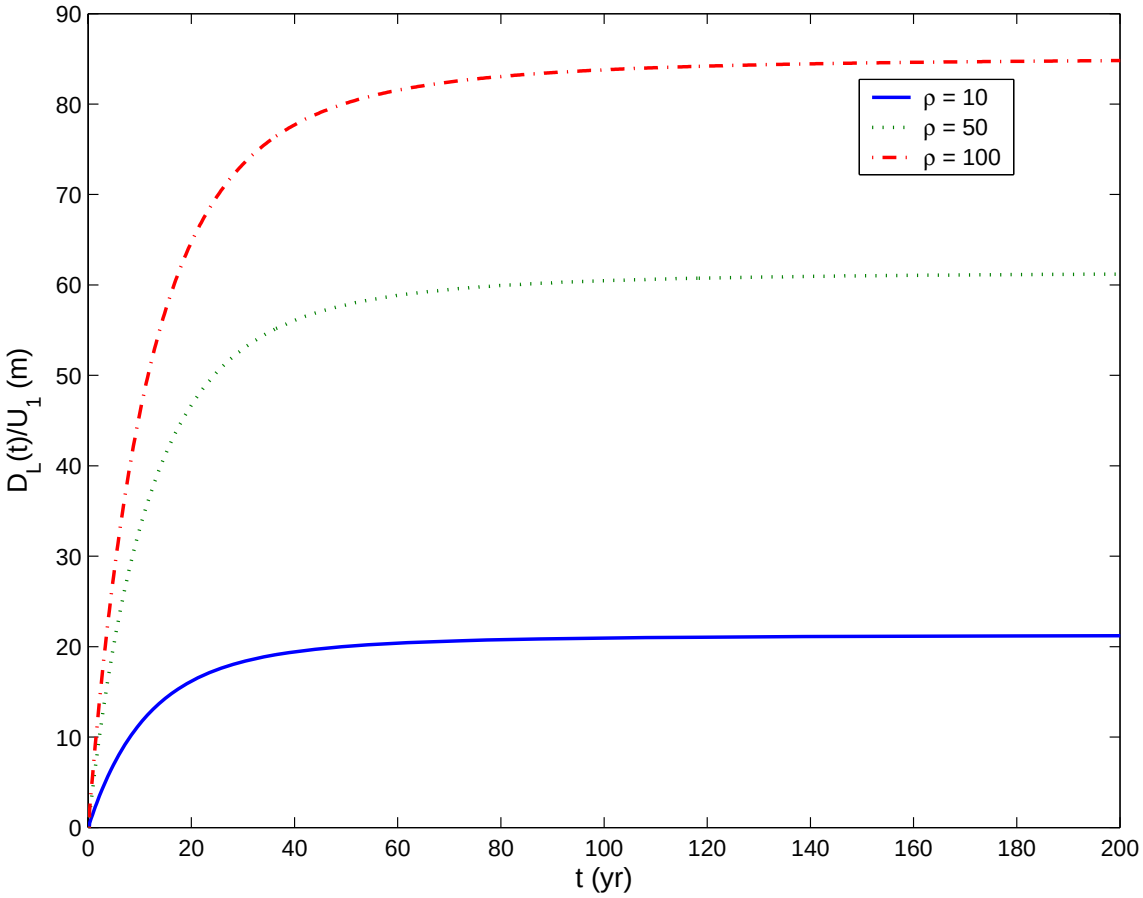

Figure 15. Level I longitudinal macrodispersitivity as a function of travel time, *t*, and ratio of geometric mean conductivity, ρ, between OFG (open-framework gravels) and non-OFG regions within the braid-belt facies.

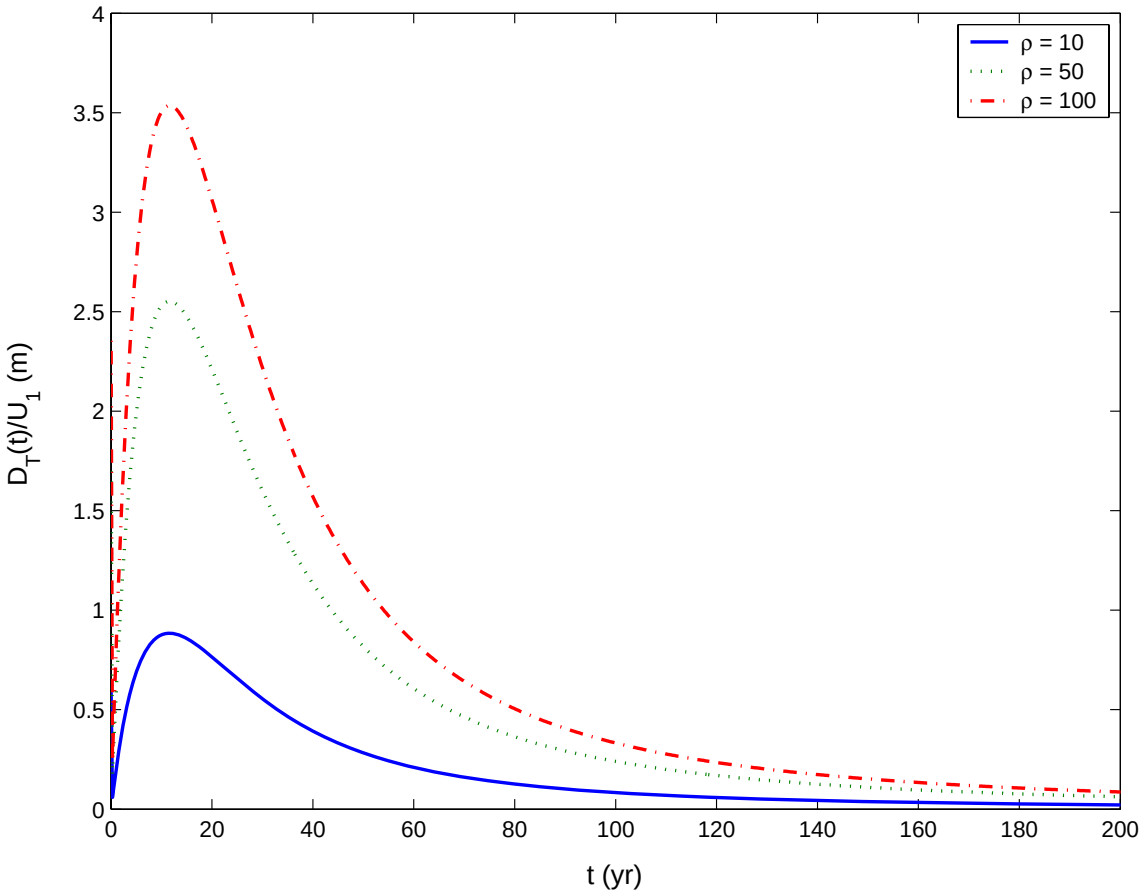

Figure 16. Level I transverse macrodispersitivity as a function of travel time, *t*, and ratio of geometric mean conductivity, ρ, between OFG and non-OFG regions within the braid-belt unit type.